UNIVERSITY OF WEST BOHEMIA
Faculty of Applied Sciences
Department of Cybernetics

BACHELOR THESIS
Application of CMOS Sensors in Biology

PILSEN, 2022   ANNA DĚDOVÁ

ZADÁNÍ BAKALÁŘSKÉ PRÁCE
(projektu, uměleckého díla, uměleckého výkonu)

Jméno a příjmení: **Anna DĚDOVÁ**
Osobní číslo: **A20B0585P**
Studijní program: **B0714A150005 Kybernetika a řídicí technika**
Specializace: **Automatické řízení a robotika**
Téma práce: **Application of CMOS sensors in biology**
Zadávající katedra: **Katedra kybernetiky**

Zásady pro vypracování

Details: Use of CMOS imaging sensor without optical elements for development of innovative biosensor for applications in biology.
Work description:

- Describe the benefits and limitations of CMOS technology when used without optical elements applied to imaging of biological samples.
- Adjust the available camera module with integrated CMOS imaging sensor for lens-free imaging (e.g. biological sample on microscopy glass slide in close proximity of the sensor).
- Realize graphical user interface enabling readout from image sensor and implement the necessary image processing algorithms.
- Describe the whole process in detail.

Rozsah bakalářské práce: **30 – 40 stránek A4**
Rozsah grafických prací:
Forma zpracování bakalářské práce: **tištěná**
Jazyk zpracování: **Angličtina**
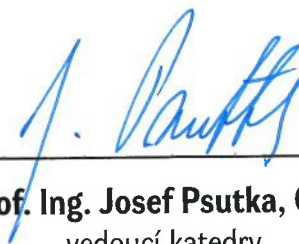
Seznam doporučené literatury:

- J. Garcia-Sucerquia et al., *Digital-Inline-Holographic microscopy*, Applied Optics 45(5), 2006
- S.K. Jericho, M. H. Jericho, H.J. Kreuzer, *Digital In-Line Holographic Microscopy in 4-D*, OSA/BIOMED/DH, 2010
- S. Barkley et al., *Holographic Microscopy with Python and HoloPy*, arXiv:1806.00058v1, eess.IV, 2018
- A. Ozcan, E. McLeod, *Lensless Imaging and Sensing*, Annual Reviews in Biomed., 2016
- J. Song et al., *Sparsity-Based Pixel Super Resolution for Lens-Free Digital In-line Holography*, 6:24681, DOI: 10.1038/srep24681, Nature, 2016

Vedoucí bakalářské práce: **Ing. Pavel Fikar, Ph.D.**
                                  Výzkumný program 1

Datum zadání bakalářské práce: **15. října 2021**
Termín odevzdání bakalářské práce: **23. května 2022**

L.S.

_____   _____
Doc. Ing. Miloš Železný, Ph.D.   **Prof. Ing. Josef Psutka, CSc.**
         děkan   vedoucí katedry

V Plzni dne 15. října 2021

Declaration

I hereby declare that this bachelor thesis is completely my own work and that I used only the cited sources.

Pilsen, May 19, 2022

Anna Dědová

Acknowledgements

I would like to thank my supervisor Ing. Pavel Fikar Ph.D. for consistent support, guidance and feedback during this project.

Abstract

With the advances in CMOS technology, the pixel size of CMOS image sensors is getting smaller and the sensor price lower, allowing for many applications in biomedical imaging. Following these advances, lensless imaging techniques are reaching sufficient resolution capabilities that enable their use instead of classical lens-based optical systems with the advantage of lower cost, dept-resolved imaging, large Field-of-View and high adaptability. This thesis introduces various lensless imaging methods and their applications, describes the basic holographic theory, reconstruction methods and step-by-step design of a digital lensless holographic microscope in an on-chip configuration.

Keywords: lensless imaging, digital holography, digital inline holoraphic microscopy, depth-resolved imaging

Abstrakt

S vývojem CMOS technologie dochází ke stálému zmenšování velikosti pixelu CMOS obrazových senzorů a ke snižování ceny senzoru, což umožňuje řadu nových využití v oblasti biomedicinského zobrazování. Díky těmto pokrokům dosahují metody bezčočkového zobrazování dostatečného rozlišení pro jejich aplikace namísto klasických optických systémů, s výhodami nižší ceny, zobrazování s rozlišením hloubky, většího zorného pole a vysoké přizpůsobitelnosti. Tato práce představuje řadu bezčočkových zobrazovacích metod a jejich aplikací, popisuje základní teorii holografie, metod holografické rekonstrukce a popisuje postupný návrh bezčočkového digitálního holografického mikroskopu v on-chip konfiguraci.

Klíčová slova: bezčočkové zobrazování, digitální holografie, digitální holografická mikroskopie, hloubkově rozlišitelné zobrazování

Contents

CHAPTER 1

Introduction

Advances in CMOS sensor technology have allowed developments in many fields ranging from consumer electronics to various applications in biology. If we focus on the imaging technologies in biology, we can see the emerging field of lensless imaging techniques that become a new alternative to classical lens-based optical systems.

The lensless imaging systems rely usually on simple hardware without any high-cost precision lenses and perform the imaging using software reconstruction and software analysis methods. Because of the shift from hardware to software complexity of the devices, their price tends to be much lower and, at the same time, they have several key advantages over the classical lens-based systems [1]. The classical systems have limited depth-of-field and field-of-view due to spherical aberrations of lenses, while on the other hand the lensless imaging systems are essentially limited only by the sensor dimensions, pixel size and signal-to-noise ratio of the sensor [2]. Some of the methods also allow depth-resolved imaging, making them especially suitable for large volume imaging, particle tracking, and cytometry applications [2].

This thesis mainly focuses on digital holographic methods, their physics background, resolution limitations and description of reconstruction algorithms. The design and implementation of a digital lensless holographic device is presented, using 3D printed housing, CMOS image sensor, LED coupled with metallic pinhole illumination aperture and angular spectrum reconstruction method.

The structure is as follows. First, various lensless imaging methods are described. Then a short overview of potential biological applications is presented with a focus on digital holography. After that follows an overview of the physics background on holography, laying the ground for the design of the lensless holographic device in the following chapter, including experimental results. Finally, the conclusion of the thesis is given.

Lensless Imaging

In the last few decades, there have been significant advances in semiconductor technology, which have opened new possibilities regarding alternative methods to classical lens-based microscopy. In particular, the image sensor technology has shifted from CCD sensors to widespread CMOS sensors, which have continued to decrease in pixel size and manufacturing price [3]. The pixel size has decreased bellow 1 μm in today's state-of-the-art sensors, which can be sufficient detail for some applications and might not require large magnification. On the other side, the computational power has also increased significantly in this period, which enables us to perform more demanding processing and to use so-called computational imaging [4]. In computational lensless imaging, no optical system with lenses is utilized for either imaging or magnification. Here only the raw diffraction pattern of the light scattered or emitted by the object is recorded and the object is then digitally reconstructed [2]. Computational imaging shifts the focus and complexity from hardware (lenses) to software (numerical algorithms and processing). This change of approach has many advantages as well as drawbacks that make it especially suitable for some applications and less so for others.

The benefits of lensless imaging are often much **lower cost** because the main price contributor of classical imaging systems is the optics (lenses). The image sensor itself is a relatively cheap item. In some cases, the light source can be relatively more expensive, but solutions with only LED are also possible and very cheap. Next, these systems are usually **smaller, lighter, and more robust** thanks to the absence of lenses, their cleaning, and alignment. They also enable **larger field of view** [5], independent on the obtained resolution. Some methods even enable **depth-resolved imaging** of the sample, which is not possible with classical lens-based imaging, because when the object moves from the focus by an even small distance, it is no longer resolvable.

The disadvantages naturally come with the **time and power** required

to perform the computations and also comparably **lesser image quality** compared to precision lense imaging within it's optimal boundaries [5]. This limits the use of lensless imaging in applications where high-quality image, high magnification, and resolution are needed and the field-of-view is not an issue as well as in applications with real-time observation requirements (except for methods with no reconstruction).

2.1 Approaches to Lensless Imaging

The approaches to lensless imaging differ greatly according to the principles that they are based on, but the device setup stays mostly similar to the one in figure 2.1. The position of the sample relative to the light source and the sensor can vary and for some methods and it can also be desirable to place the sample close to the light source to achieve greater magnification (in classical holography). The type of light source also varies depending on other requirements (mainly level of spatial and temporal coherence) from simple LED, LED with pinhole and filter, laser coupled to optical fiber, and many others. Some of the different approaches to lensless imaging are described in the following sections.
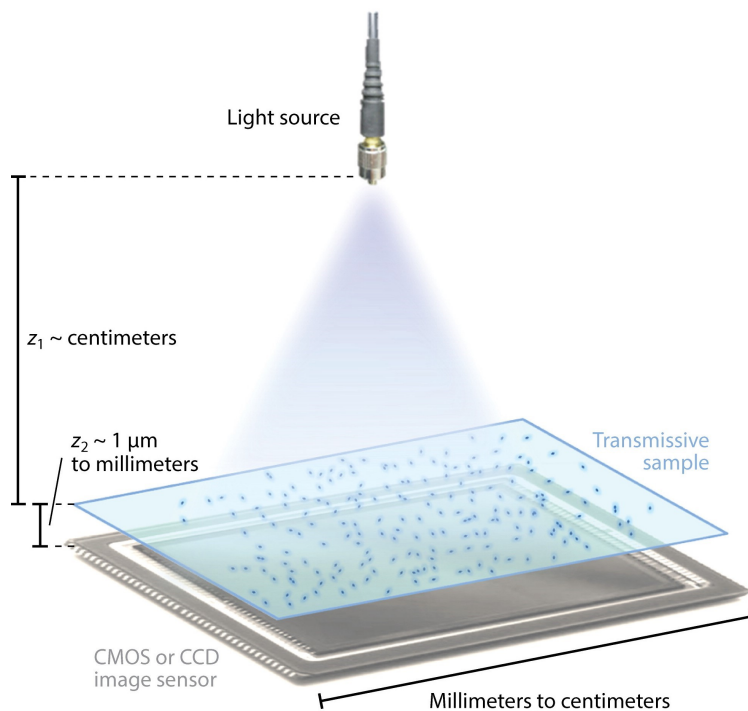

Figure 2.1: Setup of lensless imaging device [2]

2.1.1 Shadow Imaging

Shadow imaging is the simplest form of lensless imaging, where no subsequent reconstruction is performed after the recording of the image. The setup consists of a light source at distance z_1 from the sample, which is placed at a distance z_2 from the sensor. The light scattering of the sample is affected by diffraction over the distance z_2, which has a negative impact on the imaging quality. When any incoherent light source is used (which is preferred [6]), it results in blurring of the image, distorting the shape of the objects and worsening the resolution. If the light source is coherent (laser diode) or partially coherent (LED), then an interference pattern appears, which can be useful for reconstruction in holography, but without reconstruction, it creates patterns, that do not resemble the real shape of the object. [2]

Therefore in shadow imaging, it is desirable to minimize distance z_2 to achieve the best possible image quality. The ideal distance is on the order of tens of μm, the maximal useful distance is around a few mm. [2].

Because of the lesser or distorted image quality, shadow imaging is often used in a pattern matching way, where the goal is to identify some specified objects to count or track them and they do not necessarily need to resemble their real shape. [2]

An illustration of shadow imaging is shown in figure 2.2, where the shadow image, taken from distance $z_2 = 0.2\,mm$, is compared to an image taken with a 4x microscope objective.
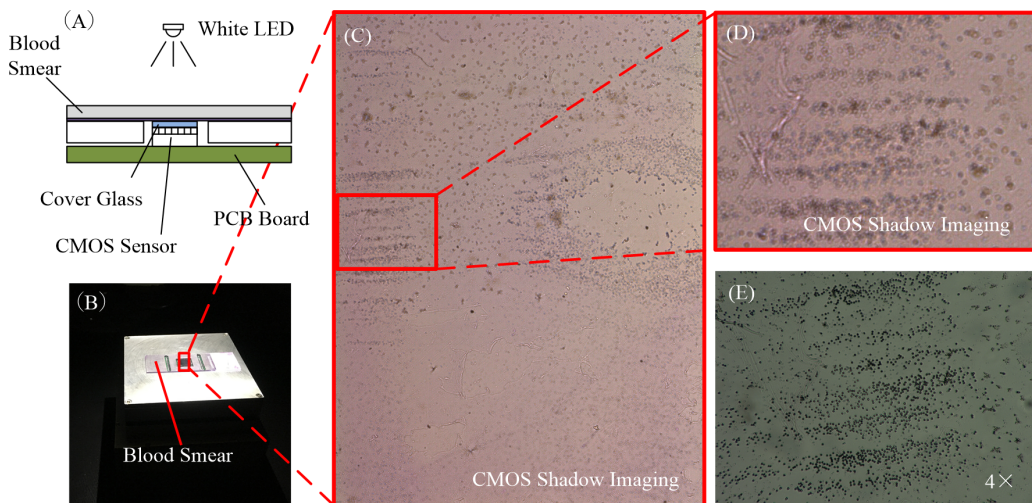

Figure 2.2: Shadow imaging of blood smear [7]

Shadow imaging is commonly used in lab-on-a-chip applications, with the sensor placed close to the sample ($z_2 \leq 0.5\,mm$). The main benefits are the low cost and wide FoV compared to a classical lens-based microscope. [5]

The resolution is limited by the pixel size and diffraction over the distance z_2 but can be improved by superresolution methods, such as combining sub-pixel shifted images of objects that are flowing over the sensor. [5]

2.1.2 Fluorescence Imaging

The lensless fluorescence imaging has a slightly different structure since the actual light emitter is the sample itself. In place of the usual light source, there is an excitation light of specified wavelength [2]. This induces fluorescence of the sample that is then captured by the image sensor, so the image is no longer the result of scattering as before.

One problem with fluorescent imaging is the need to filter out the excitation wavelength. Even after using a filter, signal-to-noise (SNR) can still be high, which can be a limiting factor to resolution. The next problem is that by using the filter, the minimal realizable distance z_2 between the sample and sensor is increased (min z_2 with filter $\approx 200\,\mu m$), which due to the diffraction worsens the achievable resolution (best achievable point spread function (PSF) $\approx 200\,\mu m$). [2]

This resolution limit is too low for most biological applications, so several ways have been explored to suppress the effect of diffraction. The critical distance z_2 can be decreased by using a sensor with a filter placed directly on the pixels. For a $6\,\mu m$ thick custom made filter, on a $5.2\,\mu m$ thick sensor, a resolution of $13\,\mu m$ has been achieved [8]. The next approach to limit the effect of diffraction is by using the tapered faceplate placed directly in between the sample and sensor. This element consists of a bundle of optical fibers that enlarge towards the sensor, magnifying the captured image and increasing resolution, achieving resolution up to $4\,\mu m$ [9]. The next way of improving the resolution is by using a mask that modifies the point spread function of the setup. The mask modulated recording is then rapidly reconstructed, achieving sub-pixel levels of resolution [10] (more details in section on mask modulated systems). Apart from other hardware improvements, there are also ways of improving the resolution computationally, via deconvolution, compressive decoding, etc. [2]

Illustration of lensless fluorescent imaging with a tapered fiber-optic faceplate is shown in figure 2.3.
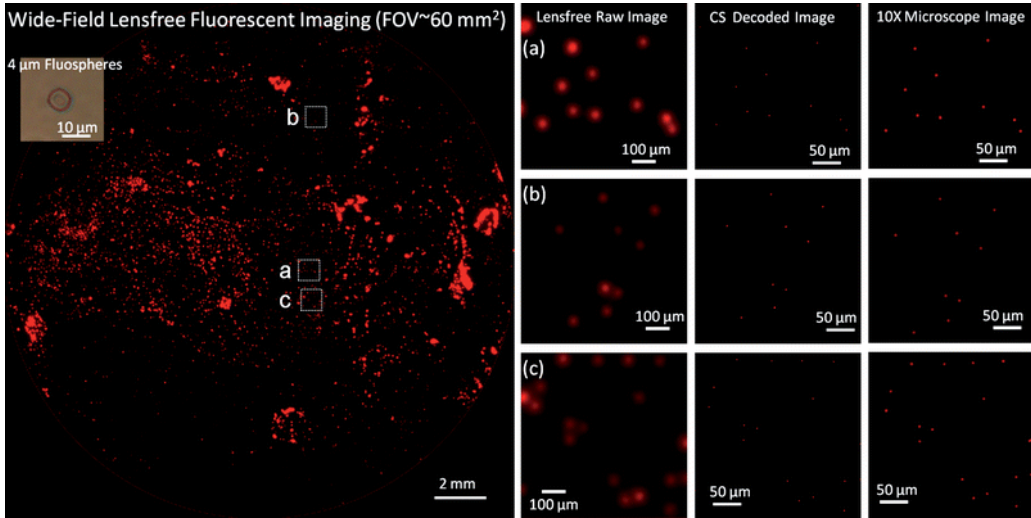
Figure 2.3: Fluorescent imaging [9]

2.1.3 Time-Resolved Lensless Imaging

The next technology of lensless imaging is time-resolved sensing. This technology uses a single laser beam to illuminate an object and directly measure the time of detection of the reflected light with a 2D array of highly time-sensitive photodetectors (time of flight depth camera). These cameras are considered a broader version of LIDAR technology. [11]

However, to this date, this technology is proven mostly only by simulations or with expensive and complicated equipment. [5]

2.1.4 Digital Holography

Digital holography is the ideal technique for achieving a wide field-of-view as well as a relatively high resolution at the same time [12], while using comparably simple hardware (in most cases). For this reason, it is often used as the preferred way for lensless microscopy and it was also chosen as the focal point of this thesis.

The merit of holography (in the sense of holographic recording) is in capturing both the **amplitude** and the **phase** of the optical wavefront at the sensor plane. This is different from shadow imaging, where only light intensity can be captured. This advantage has two main implications, firstly it allows us to reconstruct the object in a third dimension (depth) when the properties of the original light wave are known. Secondly, it allows us to observe even some objects that are transparent, because these objects may have different optical properties when it comes to absorption of light

13

and when it comes to phase modification of the light coming through the object. These properties are characterized by the refractive index, which is a complex number, where the imaginary part corresponds to the absorption of the incident wave's energy (which can be observed by measuring intensity) and the imaginary part corresponds to its phase modification [13].

History

Although capturing the complete information about the optical wavefront (both amplitude and phase) is obviously ideal, it is (or was) rather complicated task. The phase of light changes rapidly depending on its wavelength resp. frequency. Visible light wavelengths range between $400\ nm$ and $750\ nm$ and if we consider other types of electromagnetic waves that are used in microscopy, we can go even significantly below this threshold. This means, that the frequency at which the observed electromagnetic field oscillates are too high for measuring the changes in phase directly and only the intensity (time-averaged quantity) can be measured by a 2D array of detectors [14]. A novel approach to measuring the phase of incident light was proposed by Dennis Gabor in 1948 in his New microscopic principle [15] and became the foundation of holography.

Gabor's Invention

The original motivation for the invention of holography was the limitations of the electron microscopy resolution imposed by the spherical aberration of electron lenses. By emitting them from the microscope design, this limitation could be overcome. The proposed design allows recording of both the amplitude and phase in a one-step process - thus the name holography (meaning whole from Greek "holos").

This is achieved by using a **coherent** light source, which is placed inline with the object of interest and the recording photographic film (nowadays using CMOS or CCD image sensor instead). The sufficient coherence of the light source is crucial for the imaging performance, as it can limit the achievable resolution. In the original setup, the object is placed close to the light source and further from the recording medium to leverage the possible magnification given by the divergence of the spherical wavefront propagating from the point source (this is however not necessary and even systems with no magnification are used today with different benefits).

The key principle of holographic imaging is that in this setup there occurs a phenomenon known as **interference** of the reference wave (mostly undisturbed part of the wavefront passing around or through the object) and

the object wave, which is affected by the object and has different amplitude and phase (and carries all the information about the object). The resulting interaction of these two electromagnetic waves is a superposition of both, creating an interference pattern at the recording medium. This recorded pattern can be very different from the real shape of the object, but knowing the properties of the reference wave (wavelength and geometry of the setup), the object wave in the arbitrary distance can be reconstructed (optically or numerically).
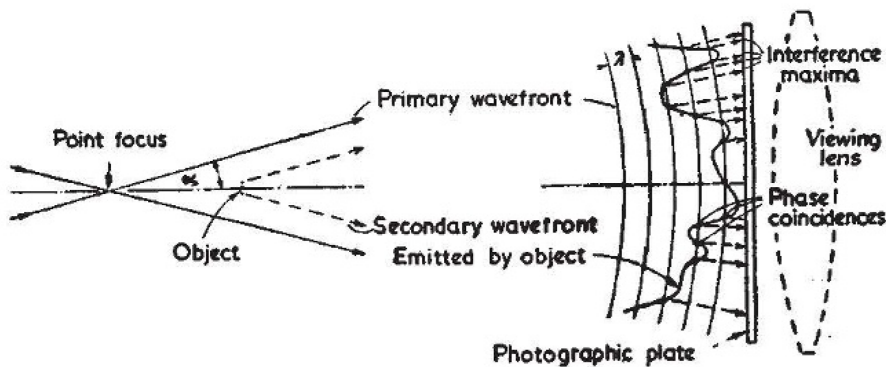

Figure 2.4: Original schema of Gabor's hologram recording [15]

Comparison to Classical Lens-based Microscopy

The compound microscope (or light microscope) is the most used and the most traditional microscopic imaging device in many fields. Because of its reliance on lenses, it has a few limitations that do not exist with lensless imaging.

The first characteristic of lens-based imaging is its trade-off between the resolution and field-of-view. Using a lens system with a higher numerical aperture and better resolution results in a decrease in field-of-view (FOV is inversely proportional to the magnification squared [16]). This does not hold for lensless systems, where the FOV, although also decreased by increasing magnification, can be independently adjusted simply by using a sensor with a larger area or pixel density.

Secondly, the depth-of-field of lens-based systems is also very narrow, limiting their use to thin samples and problematic for imaging of larger volumes [17]. However, in digital holography by using the information about light propagation, described by the physical properties and geometry of the light source, we can refocus at any plane perpendicular to the sensor. Resolution in the axial direction is admittedly worse than the lateral resolution

15

[2], but this does not limit the dept-of-field and every single image can be digitally refocused to any depth.

Lastly, in the compound microscope, the lens system contributes to the majority of cost and weight that can be completely reduced by using lensless imaging techniques [5].

As for the benefits of lens-based microscopy over digital holography, mainly the reconstruction process is a big drawback, compared to instant optical reconstruction by the compound microscope.

Also, the noise present in holographic reconstructions negatively impacts the resulting quality. In the quality aspect, the lens-based imaging is superior to digital holography [5].

Another difference is that digital holography is inherently monochromatic. The color imaging is possible but requires hardware adjustments and additional image processing [18].

State-of-the-art DIHM

The performance and design of digital inline holographic microscopy (DIHM) devices differ depending on the objective of their application. The focus can be either on wide field-of-view and imaging volume, on the best possible lateral resolution, 3D imaging and tomography, cost, size, or other aspects.

Devices for these different priorities have different construction, which can range from a simple laser diode above the sample and sensor to multiple light sources at different angles, moving parts, such as scanning platforms, or sources at different wavelengths. The cost can vary accordingly from 52.82 USD [17] (in figure 2.5) to devices including more sophisticated laser sources and other devices in the different price ranges.

As for the resolution, diffraction limit ranging resolution can be achieved with the original design of holography with a laser light source and sample closer to the light source. However, holography with highly coherent light sources suffers from speckle artifacts [2]. The preferred design, for avoiding this issue is using partially coherent light sources with the sample placed close to the sensor and close to no magnification [2]. With this design, the resolution is limited by the size of pixels which is around $1\mu m$ in today's best sensors. This can be to some extent surpassed by either software superresolution algorithms based on signal processing methods [19] or by combining multiple shifted images or possibly scanning from different angles [20]. This way, by using synthetic aperture, resolution on a level of 250 nm was achieved even in on-chip microscopy, but with a considerably complicated setup (in figure 2.6)[20].
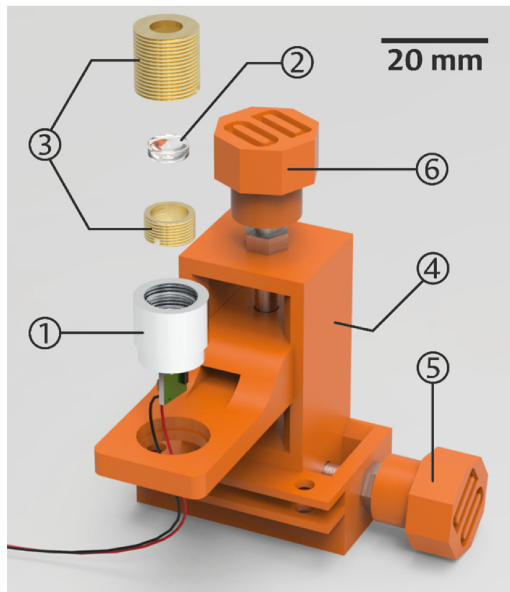
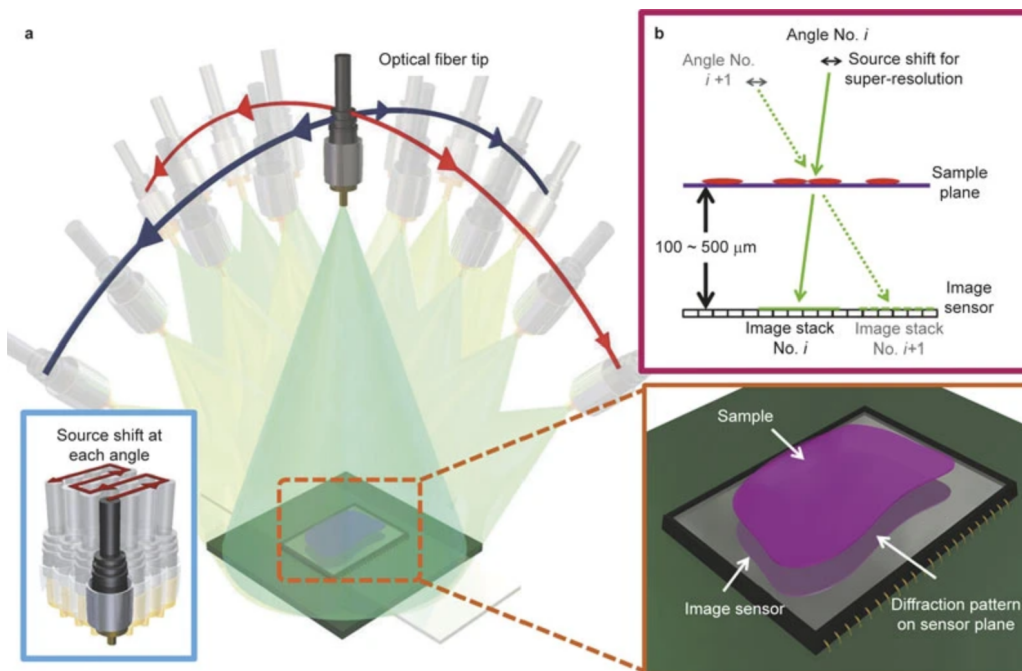Figure 2.5: Cost-effective, 3D-printed DIHM [17]

Figure 2.6: Synthetic aperture-based on-chip microscopy [20]

2.1.5   Mask Modulated Lensless Systems

Apart from illumination modulated lensless systems, where the illumination is the key for the performance of the system and possibly for image reconstruction (holography, time-resolved sensing, shadow imaging, etc.), there is also one different category - mask-modulated lensless systems.

The mask modulation consists in designing a transfer function that modifies the light field in such a way that even it's high-frequency components can be detected by the sensor array and from this measurement, the original light field can be inversely reconstructed in high detail. [16]

This transfer function is implemented by a thin film - amplitude or phase mask, placed on top of the sensor array. After the mask is fabricated, the precise model parameters are identified (calibrated) and the model is then used for rapid reconstruction.

The mask modulated and illumination modulated systems are similar in principle, that is both are modulating the light field so that the sensor is capable of recording the useful information that would otherwise be at high frequencies. High frequencies above the sampling limit are otherwise impossible to be recorded by the image sensor with limited pixel size (sampling). However, the light modulation (mainly holography), though more traditional and proven in microscopy, has its limitations in its reliance on coherence (which depends on both distance from the light source and its temporal coherence). Mask modulation on the other way can be used at larger distances as well as in applications, where no temporally coherent light source is a possibility (fluorescence imaging, in vitro and in vivo imaging) [16]. It is also the most compact the lensless imaging technique, with devices as thin as 1 mm and reaching resolution of less than $2\,\mu m$[16].

Biological Applications of Lensless Imaging and Sensing

The lensless imaging systems have advantages over classical lens-based systems in several areas that are key for their applications. Lensless imaging devices are suitable for applications where low-cost diagnostic is needed or a large volume or large Field-of-View samples need to be analyzed. These devices are also suitable for tracking or imaging moving objects, for example in micro-fluidic channels [21] and to some extent 3D tomographic imaging.

They are usually not suitable for applications where real-time observation or high-quality imaging is required. For this purpose, lens-based imaging systems are mostly superior [2]. Another limitation (for holographic methods), is its inability to image dense or largely opaque samples (for example tissues).

3.1 Point-of-care and Customized Imaging

The major advantage of lensless imaging systems is their low cost, easy customization, and small dimensions [22]. As such, these imaging systems can be integrated with microfluidic channels to perform analysis and decision-making tasks [22] and integrated into point-of-care diagnostic systems.

The price of the system varies according to the complexity of the setup, but for basic 3D printed DLHM devices, the price is mainly dependent on the cost of the imaging sensor and the pinhole (or other aperture), starting from 190 USD for the complete imaging setup [17].

As an example of a more complex device utilizing superresolution techniques, an on-chip lensless imaging device was reported achieving $1\,\mu m$ resolution for 600 USD, enabling tracking of human sperms in microfluidic channels [22].

3.2   Particle Tracking

Digital holography is a very convenient method for tracking of particle movements in 3D environment [23]. The complete information about the object at any single point in time is captured by a single image and by recording a series of holograms (capturing a video recording), and all the 3D movement information is captured. To eliminate the stationary objects, the difference holograms are created for any two consecutive images and these images are then reconstructed in a selected stack of depths for each time [23].

This method was demonstrated in the tracking of bacteria in the Atlantic ocean [23] in an experiment, that would be hard to replicate with other lens-based methods, due to the limited Dept-of-Field and Field-of-View of the lenses.

3.3   Particle Detection

The limit for particle detection is generally much lower than the resolution limit, enabling the detection of very small particles (up to tens of nm in diameter) with lensless systems [2]. This is different from imaging, where the shape and the the relative size of the objects needs to be preserved, but the detection and sensing of particles is sufficient for many applications. An example of such use-cases is most of the statistical analysis methods for biological samples, such as the viral load measurements, etc.[2] From other fields another application can be for example in air quality monitoring [2].

3.4   3D Tomography

Although digital holography is an ideal technique for large volume scanning and allows digital refocusing (reconstruction) of the image at different depths, the 3D imaging itself has some limitations. In the classical setup with single image digital holography, the problem of 3D object reconstruction is ill-posed [24], meaning there is more than a single solution, and therefore digital holography is not considered a tomographic method. However, a 3D image can still be estimated by eliminating the twin image (complex conjugate) [24] using any of the methods described in section 4.2.4. These can utilize either assumption about the object position and shape or multiple measurements at several heights or angles.

Another important issue for the lensless tomographic microscopy is the difference between lateral and axial resolution obtained with different illu-

minating setups. With single angle illumination, for the sub-micron lateral resolution, the axial resolution is still around $45-50\,\mu m$ [25]. Significant improvement in axial resolution has been shown using multi-angle illumination scanning of the sample using 24 LEDs coupled to optical fibers, reaching axial resolution of less than $7\,\mu m$ [25]. Even better resolution $1\,\mu \times 1\,\mu \times 3\,\mu m$ was demonstrated using a setup with two axes of illumination rotation and multiple subpixel shifts at every angle [26].

In conclusion, digital holography can be used for 3D imaging, but requires more complicated hardware setup and image processing algorithms in order to reach a reasonable axial resolution.

Theoreticall Fundamentals of Digital Holography

4.1 Physics Background

Before describing the theory of digital holography, the most relevant parts of optics and wave propagation are introduced in following sections.

4.1.1 Light Waves

The description of waves comes as a solution $\psi(x,t)$ to the differential wave equation (4.1) that describes its motion and is a function of both time and space. [27]

$$\frac{\partial^2 \psi}{\partial x^2} = \frac{1}{v^2}\frac{\partial^2 \psi}{\partial t^2} \tag{4.1}$$

This equation holds for a one-dimensional description of both moving particles or other waves such as propagating electromagnetic fields.

The lightwave propagation can be described both as oscillating particles (photons) or as an oscillating electromagnetic wave and both of these models are being used for the description of different phenomena. For the sake of digital holography, the most important phenomena are interference and diffraction, which are both best described by the wave model (by the theory of electromagnetism). In optics, the field used to describe the wave is usually the electric field $\vec{E}$, described by **partial differential wave equation** (4.2), derived from Maxwell's equations. [14]

$$\nabla^2 \vec{E} - \frac{1}{c^2}\frac{\partial^2 \vec{E}}{\partial t^2} = 0 \tag{4.2}$$

where ∇^2 is the Laplace operator: $\nabla^2 = \dfrac{\partial^2}{\partial x^2} + \dfrac{\partial^2}{\partial y^2} + \dfrac{\partial^2}{\partial z^2}$

The solution to equation 4.2 is given by expression 4.3, where $E(x, y, z, t)$ is a description of electric vector field at point $\vec{r}$ in space and time t.

$$E(x, y, z, t) = a \cos(\omega t - \vec{k}\vec{r} - \varphi_0) \tag{4.3}$$

The vector $\vec{k}$ is called the wave vector and describes the direction and velocity of spatial wave propagation (Eqn. 4.4). The vector $\vec{n}$ is the unit vector in the direction of spatial propagation.

$$\vec{k} = k\vec{n} = \frac{2\pi}{\lambda} \cdot \vec{n} \tag{4.4}$$

The angular frequency of lightwave ω is given by its frequency $\omega = 2\pi f$, resp. by wavelength $\omega = 2\pi \frac{c}{\lambda}$, where c is the speed of light. The amplitude of the wave is denoted as a.

The cosine function describing the electric field can be decomposed to temporally varying part ωt and spatially varying part $\varphi = -\vec{k}\vec{r} - \varphi_0$, defined as the phase. In the complex form, the wave can be represented by eqn. 4.5, where the temporal and spatial parts are separated. [14]

$$E(x, y, z, t) = a \cdot e^{i\omega t} \cdot e^{i\varphi} \tag{4.5}$$

In calculations concerning holography, only spatial distribution of the electric field is of importance and this is described by so called **complex amplitude** $A(x, y, z)$ (eqn. 4.6). [14]

$$A(x, y, z) = a \cdot e^{i\varphi} \tag{4.6}$$

Since the light field is not directly measurable, the measured quantity is the **intensity**. The intensity is proportional to the time average of the square of the electrical field (Eqn. 4.7) and the square of the modulus of the complex amplitude (Eqn. 4.8). [14]

$$I = \epsilon_0 c \lim_{T \to \infty} \frac{1}{2T} \int_{-T}^{T} E^2 \, dt \tag{4.7}$$

$$I = \frac{1}{2}\epsilon_0 c|A|^2 = \frac{1}{2}\epsilon_0 c A^* A \sim |A|^2 \tag{4.8}$$

$$I = \frac{1}{2}\epsilon_0 c a^2 \tag{4.9}$$

4.1.2 Interference

Interference is a **superposition** of two or more waves in space and is a very important phenomenon leveraged in the holographic recording. To create a static intererence pattern, the waves need to be **coherent**, meaning that those waves have the same frequency (wavelength) and shape.

If we consider two monochromatic waves A_1 and A_2 with different amplitudes and phases, the resulting complex amplitude A is their sum.

$$A_1(x, y, z) = a_1 e^{i\varphi_1} \tag{4.10}$$

$$A_2(x, y, z) = a_2 e^{i\varphi_2} \tag{4.11}$$

$$A = A_1 + A_2 \tag{4.12}$$

The created intensity pattern is of interest to holographic theory, because it captures the phase difference of both waves.

$$
\begin{aligned}
I &= A \cdot A^* \\
&= (a_1 e^{i\varphi_1} + a_2 e^{i\varphi_2}) \cdot (a_1 e^{-i\varphi_1} + a_2 e^{-i\varphi_2}) \\
&= a_1^2 + a_2^2 + 2a_1 a_2 \cos(\varphi_1 - \varphi_2) \\
&= I_1 + I_2 + 2\sqrt{I_1 I_2} \cos \Delta\varphi
\end{aligned}
\tag{4.13}
$$

The last term of expression 4.13 is the interference term and depends on the phase difference $\Delta\varphi$ of both waves. The resulting pattern consists of periodically and equidistantly spaced brighter and darker fringes at places of constructive (Eqn. 4.14) resp. destructive (Eqn. 4.15) interference and varying intensity in between.

$$\Delta\varphi_{max} = 2n\pi \qquad n \in Z^+ \tag{4.14}$$

$$\Delta\varphi_{min} = (2n + 1)\pi \qquad n \in Z^+ \tag{4.15}$$

The **fringe spacing** d is an important parameter for the resolution of the hologram. It is defined as the distance of two consecutive interference maxima and can be derived from the geometry of two interfering waves at different angles of propagation. The resulting distance is given by equation 4.16, where θ is the angle between the propagating directions of both waves and λ is their wavelength. [14]

$$d = \frac{\lambda}{2 \sin\left(\frac{\theta}{2}\right)} \tag{4.16}$$

4.1.3 Diffraction

Diffraction occurs when the wavefront encounters an obstacle that becomes a source point of secondary waves. The obstacle can be both transparent and opaque, changing either amplitude or phase of part of the wavefront [27]. The wavefield after the obstruction is constructed by the interference of different wavefront segments, creating a **diffraction pattern**.

Interference and diffraction refer to the same physical phenomena, but interference is usually referred to when the interaction of two or a few more waves are considered and diffraction when considering a large number of interfering waves (created from one original wavefront). [27]

The diffraction can be explained by classical optics, by the **Hyugens-Fresnel principle**. Every point of the unobstructed wavefront is considered a source of spherical secondary wavelets and the amplitude of the optical field after the obstruction is the coherent superposition of all of these wavelets (considering both their amplitude and relative phases). [27]

The mathematical description of diffraction is given by the **Fresnel-Kirchhoff integral** (Eqn. 4.17), where $A(x, y)$ is the complex amplitude in the observation plane, $A_0(x_0, y_0)$ is the complex amplitude of the aperture (obstacle), r is the distance between a point in the aperture plane and a point in the observation plane, z is the distance between the source plane (aperture) and observation plane. The integration is overall secondary spherical waves, emerging from the aperture plane. The factor Q restricts the waves from traveling backward. It depends on the angle θ between the normal vector $\vec{n}$ to the aperture plane and angle of incident light from the source and the angle θ' between the diffracted light and $\vec{n}$. In realistic scenarios, the factor $Q \approx 1$. [14]

$$A(x, y, z) = \frac{i}{\lambda} \int_{-\infty}^{\infty} \int_{-\infty}^{\infty} A_0(x_0, y_0) \frac{e^{-i\frac{2\pi}{\lambda}r}}{r} Q \, dx_0 dy_0 \qquad (4.17)$$

$$r = \sqrt{(x_0 - x)^2 + (y_0 - y)^2 + z^2}$$
$$Q = \frac{1}{2}(cos\theta + cos\theta')$$

The diffraction phenomenon is most noticeable if the dimensions of the obstacle are on the order of the wavelength of the incident light. [14]

4.1.4 Coherence

For the interference to occur, the important condition is the coherence of interacting waves. By definition, any two waves are (completely) coherent if they have the same frequency and waveform (shape). However, real light sources are usually only **partially coherent** or incoherent.

For practical reasons, the concept of coherence is further divided in temporal and spatial coherence.

The **temporal coherence** means coherence of the wave in time - how long can we reasonably predict the phase of the lightwave at a given point in space [27]. It is related to the light source's frequency bandwidth Δf. The time for which the wave is coherent is called the **coherence time** $\Delta t_c = \frac{1}{\Delta f}$. The more coherent the light source is, the larger the coherence time.

The **spatial coherence** describes the coherence of two different points in space. If the two points at the same distance from the source are at a distance z from each other, then if z is smaller than the **coherence length** $L_c = c \cdot \Delta t_c$ those points are considered part of the same wavefront with the same phase. Further spaced points would have their phases unrelated. This property is also connected to the spectral bandwidth and the dimensions of the light source. [27]

Mathematically, the coherence respresents the autocorrelation of the electric field and is described by the complex self-coherence funtion $\Gamma(\tau)$ (eqn. 4.18). [14]

$$\Gamma(\tau) = \lim_{T \to \infty} \frac{1}{2T} \int_{-T}^{T} E(t + \tau) E^*(t) \, dt \qquad (4.18)$$

Fringe visibility

The fringe visibility V describes the measure of contrast between two consecutive interference maxima and minima (their intensity). The visibility of fringe pattern at point $\vec{r}$ in space is given by equation 4.19. [14]

$$V(\vec{r}) = \frac{I_{max} - I_{min}}{I_{max} + I_{min}} \qquad (4.19)$$

If the two waves were completely coherent, then by subsituting the conditions for constructive interference I_{max} from eqn. 4.14 and for destructive interference I_{min} from eqn. 4.15 to equation for intensity (4.13) would give:

$$V_{coherent} = \frac{2\sqrt{I_1 I_2}}{I_1 + I_2} \qquad (4.20)$$

4.2 Fundamentals of Holography

4.2.1 Principle of Holography

As mentioned before, the goal of holography is to record the **complete information** about the optical wavefront at the object including its phase. Because it is impossible to measure the phase directly, the way holography achieves this by utilizing interference between a known **reference wave** and the **object wave** scattered from the object. Interaction between these two waves creates an interference pattern, encoding the information about phase into the fringe spacing and intensity.

From this principle follows, that in the holographic recording, the reference wave must always be at least **partially coherent** in order to create the interference pattern with the scattered wave.

After taking the hologram, the original object wavefront can be **reconstructed** either numerically or optically (in analog holography). Numerical reconstruction can be performed on the computer by any of the methods described in section 4.2.3. For this kind of reconstruction it is needed to have digitally recorded hologram (by the CCD or CMOS image sensor) and to know the properties of the reference wave. The optical (analog) reconstruction on the other way can be performed manualy using the same reference light that was used for taking the hologram. The hologram in this case is recorded on a thick photographic film. To reconstruct, the film is illuminated from the same position as before and the observer now sees a 3D object from the recording behind the hologram. [28]

4.2.2 Digital In-line Holographic Microscopy

Digital (lensless) in-line holographic microscopy (DIHM) uses the simplest of holographic setups. In this setup, the object is placed on the optical axis between the light source and the sensor (hence inline), shown in figure 4.1.
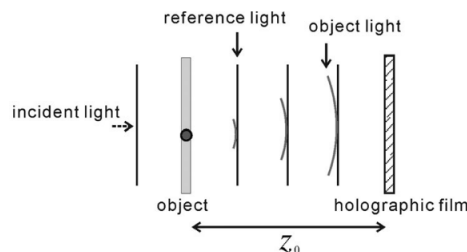

Figure 4.1: Setup of DIHM recording [29]

The reference wave $R(x, y, z)$ is created by the illumination source. Assuming the sample is not too opaque and not exceedingly large, we can consider the reference wave as largely unscattered for the sake of reconstruction. This assumption is however a limiting factor to the range of applications of this kind of holographic setup. [30]

The small part of the reference wave that gets scattered is called the object wave $O(x, y, z)$ and if the illumination is sufficiently coherent, both of these waves interfere and create an interference pattern (hologram). [30]

The hologram intenstity $E_0(x_0, y_0, 0)$ is expressed mathematically in equation 4.22.

$$E_0 = |R + O|^2 \tag{4.21}$$
$$E_0 = |R|^2 + |O|^2 + R^*O + RO^* \tag{4.22}$$

In Eqn. 4.22, the term $|R|^2$ resembles mostly uniform illumination intensity, which can be ignored or subtracted before the reconstruction [31] and carries no information about the object [30]. The term $|O|^2$ is the self-interference of the scattered wave. This term is negligible because the sample is assumed to be only weakly scattering in this setup. The next two terms are the most important because they carry the information about the sample and at the same time they are much stronger than the $|O|^2$ term. They resemble the holographic diffraction pattern [31] and after the reconstruction, they represent the object wave, resp. it's a complex conjugate.

Because of the complex conjugate image, there arises a phenomena called twin image [30], which can negatively impact the quality of inline holographic reconstruction in some cases. This is illustrated with a schema of analog (optical) reconstruction of in-line hologram in figure 4.2, where the observer sees two reconstructed images in the opposite direction from the recording plane.
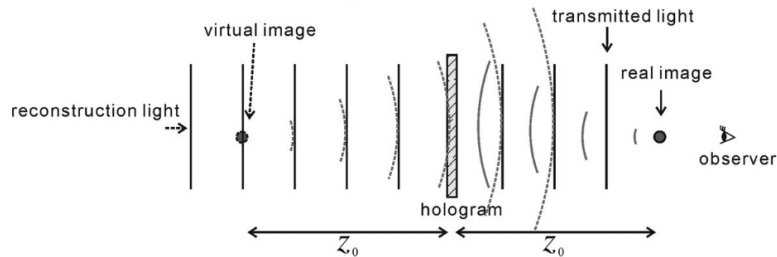

Figure 4.2: Analog reconstruction of in-line hologram [29]

4.2.3   Digital Holographic Reconstruction

In digital holography, the way of reconstructing the object image is principally similar to analog reconstruction, where it is done by illuminating the hologram with reconstruction light. Here we illuminate the recorded hologram matrix virtually and propagate the light wave back from the sensor to the object plane [30]. The differences between the algorithms are in the way propagation is computed to calculate the complex amplitude at a specified distance (sensor to object distance). Preferably both phase and amplitude images are computed in the reconstruction. [30]

The wave propagation is described by the theory of diffraction and can be mathematically described by either Fresnel-Kirchhoff integral (Eqn. 4.17) or Rayleigh-Sommerfeld diffraction integral.

Fresnel Propagation Method

The first method, the Fresnel propagation, uses Fresnel approximation to express the complex amplitude of electric field $E(x, y, z)$ in distance z from the sensor plane (eqn. 4.23) [30]

$$E(x, y, z) = \frac{i}{\lambda z} e^{-i\frac{2\pi}{\lambda}z} \int_{-\infty}^{\infty} \int_{-\infty}^{\infty} E_0(x_0, y_0, 0) \cdot e^{-i\frac{\pi}{\lambda z}r} \, dx_0 \, dy_0 \qquad (4.23)$$

$$r = (x - x_0)^2 + (y - y_0)^2$$

where λ is the wavelength of the reference wave, (x, y) are the coordinates of a point in the propagated object plane, z is the propagation distance, $(x_0, y_0, 0)$ are the coordinates of a point in hologram plane and E_0 is the complex amplitude in the hologram plane. [30].

The problem with this method is, that it uses an approximation of the propagation geometry so that a fast Fourier transform can be used for its computation. For this either an assumption is made that the distance between the light source and object is much smaller than to the screen or vice-versa. [32] As a result of this approximation, the resolution of the output image is decreased.

The reconstruction can also be improved by creating a contrast image from the hologram before the reconstruction. This is done by subtracting the background image (with no sample) from the hologram and compensating for the non-uniformity and imperfections of the illumination source. [32]

Angular Spectrum Method

A more accurate way of reconstructing the image is using the description of wave propagation by Rayleigh-Sommerfeld diffraction integral (Eqn. 4.24) without approximations. [30]

$$E(x, y, z) = \int_{-\infty}^{\infty} \int_{-\infty}^{\infty} E_0(x_0, y_0, 0) \cdot \frac{e^{i\frac{2\pi}{\lambda}r}}{r} \cdot \frac{z}{r} \left(\frac{1}{2\pi r} + \frac{1}{i\lambda} \right) dx_0 \, dy_0 \quad (4.24)$$

$$r = \sqrt{(x - x_0)^2 + (y - y_0)^2 + z^2}$$

where λ is the wavelength of the reference wave, (x, y) are the coordinates of a point in the propagated object plane, z is the propagation distance, $(x_0, y_0, 0)$ are the coordinates of a point in hologram plane and E_0 is the complex amplitude in the hologram plane. [30].

Because this integral can be rewritten also as a **convolution**, we can compute it using **angular spectrum method**. Let's denote $h(x, y, z)$ as impulse response of the free space propagation (exp. 4.25).

$$h(x, y, z) = \frac{e^{i\frac{2\pi}{\lambda}r}}{r} \cdot \frac{z}{r} \left(\frac{1}{2\pi r} + \frac{1}{i\lambda} \right) \quad (4.25)$$

Then we can express the resulting complex amplitude of propagated field $E(x, y, z)$ as in eqn. 4.26 and compute the field using Fourier and inverse Fourier transform (eqn. 4.27). This is also illustrated in figure 4.27.

$$E(x, y, z) = h(x, y, z) * E_0(x_0, y_0, 0) \quad (4.26)$$

$$E(x, y, z) = \mathcal{F}^{-1}\{\mathcal{F}\{h(x, y, z)\} \cdot \mathcal{F}\{E_0(x, y, 0)\}\} \quad (4.27)$$

The Fourier image of the impulse response of free space propagation can be expressed as

$$\mathcal{F}\{h(x, y, z)\} = e^{i2\pi f_z z} \quad (4.28)$$

where $f_z = \sqrt{\lambda^{-2} - f_x^2 - f_y^2}$ for $f_x^2 + f_y^2 \leq \lambda^{-2}$ and $f_z = 0$ otherwise. The f_x and f_y are Fourier frequencies in directions x resp. y [30] and can be determined from the pixel size and pixel count of the sensor.

Although this method uses no approximations, it was initially not preferred because of the sampling problem in the transfer function (especially for far-field propagation) [30]. This can however be overcome by limiting the bandwidth of propagation field [33].

4.2.4 Twin Image

Because the captured hologram involves both the contribution from the object wave and the from the conjugate object wave, the resulting back-propagated amplitude image involves both of these contributions. The reconstructed conjugate image does not resemble the object in the correct position (referred to as the twin image) and disturbs the image reconstruction quality. The presence of conjugate solution in wavefront reconstruction also complicates the correct estimation of the object's phase image. The way the twin image is separated and the correct phase is computed is not trivial and can be done by several different approaches. [30]

The first approach, the **phase retrieval algorithms**, uses the information about the position and shape of the object. The initial phase guess is iteratively updated by propagating the hologram to the object plane and back while restricting the reconstructed image. [34]

The next possibility is using **multi-height setup**, where the holograms are taken with different heights of the illumination source. The phase guess is again improved by propagating to different heights until the reconstructed amplitude matches at every height. No information about the object is needed in this method. [30]

It is also possible to avoid the twin image issue using **off-axis holography** setup, where the conjugate object wave can be separated based on a different angle of illumination by the object and reference beams. The reference wave, the object wave, and the conjugate object wave can then be completely separated in the frequency domain. [29]

4.2.5 Coherent vs. Partially Coherent Illumination

In the in-line holography, the main design decision is about the placement of the sample (object) with respect to the sensor and to the light source. There are two recommended approaches that differ in the hardware needed.

Highly coherent setup

First approach is to to place the sample close to the light source and far from the recording screen ($z_1 = |PO| << z_2 = |OC|$ in fig. 4.3). This is the originally intended setup Gabor proposed in his paper in 1948 [15]. Because now there is a large distance z_2 over which the object wave and reference wave need to stay coherent (in order to interfere at the sensor plane), it is necessary to use a **highly coherent light source**.
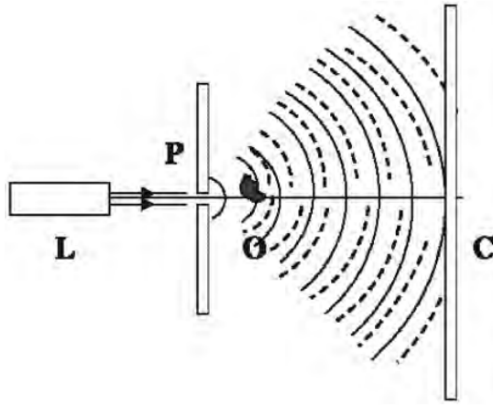
Figure 4.3: Coherent DIHM setup: L is the laser source, P the pinhole, O the object and C the recording screen [31]

Sufficient coherency is usually achieved by a laser that is focused on a pinhole of the size on the order of the wavelength [30] (there are also other possibilities for creating the point source that will be discussed later). This setup leads to **larger magnigication** of the interference pattern by propagating the diverging beam over a larger distance z_2. The magnification of the system can be computed as $M = 1 + z_2/z_1$. This enables us to increase the fringe resolution (and therefore system resolution) by magnifying the pattern on the screen and therefore avoiding the limitation imposed by the sampling of the screen (pixel size) and reaching resolution only limited by the width of the sensor [30].

However, with increased magnification there comes also decreased field of view (inversely proportional to M) [30] and by that this holographic setup loses one of the biggest advantages of lensless imaging. Highly coherent interference also causes problems with speckle noise and multiple reflections interference [30], dettering the quality of the reconstructed image. The micrometer-sized pinhole is the next difficulty because it requires precise alignment and thus more expensive mechanical and optical elements [30]. Pinholes of this size are also difficult to manufacture and their shape can be far from ideal [35], resulting in a distorted spherical wave.

Partially coherent (on-chip) setup

The second design possibility is placing the sample in close proximity to the sensor and far from the light source (fig. 4.4). This essentially gives up the possibility of magnification ($M \approx 1$), but uses the maximal field of view (entire area of the sensor) and significantly lowers the difficulty and price of
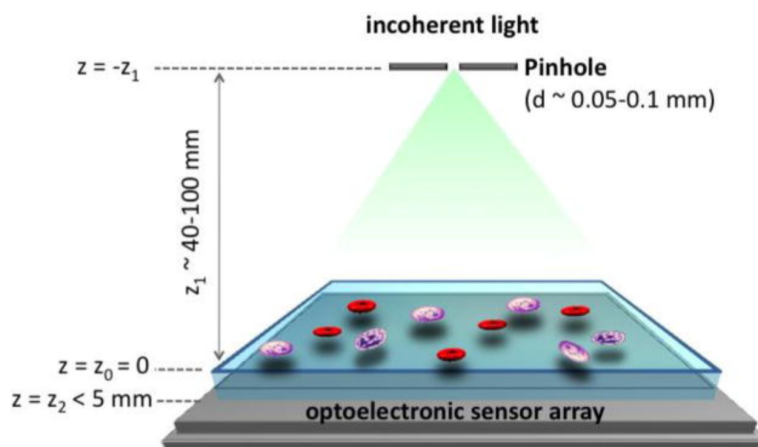
the setup. [30]

Figure 4.4: On-chip DIHM setup [36]

In this setup, since the distance between sample and sensor is small (a few μm to a few mm), the light source can be only partially coherent and still interfere on the recording screen. The pinhole can be much larger than in the previous setup (tens or hundreds of μm) and the bandwidth of the light source necessary can be achieved with LED or LED with bandwidth filter. The precise alignment of the light source and pinhole is also not necessary anymore which makes the system more robust and easier and cheaper to set up.

The next consequence of using a partially coherent light source is that it eliminates much of the speckle and reflection noise observed in highly coherent holography. The twin image on the other hand is more observable because the conjugate image is much closer to the desired image and more focused than in previous geometry. [30]

The limiting factor in this setup is ideally only the pixel size of the sensor. The state-of-the-art sensors achieve a pixel size of approx. $1\mu m$, which may not be sufficient for some applications and may require more advanced superresolution techniques. [30]

4.2.6 Limits on Resolution

Resolution

Resolution is the ability of an optical system to distinquish detail. More precisely, two point resolution is defined by the distance at which two closely spaced points can barely be resolved. The images of those two points are not

sharply bounded, but due to diffraction create patterns that overlap to some extent. Since the resolution of two objects by human eye can be subjective, the Rayleigh's criterion (eqn. 4.29) is usually used to define the separation. [37]

$$\theta \approx \sin(\theta) = 0.61 \frac{\lambda}{D} \tag{4.29}$$

The Rayleigh criterion states that two points are just resolvable if the first diffraction minimum of one point coincides with the maximum of another. [37]. In eqn. 4.29, the angle θ describes the position (angle from optical axis) of first intensity minimum and therefore half of the distance at which can two points be resolved. D is the aperture diameter and λ the illumination wavelength.

In optical systems, the resolution Δx of the system is often described by numerical aperture (NA), which relates to the maximum scattering angle θ_{max} at which light leaves the device (lens) to form an image and by n which is the refractive index of the medium. In eqn. 4.30, D is the lens diameter and d is the distance to the object.

$$\sin \theta_{max} = \frac{D/2}{d} \tag{4.30}$$

$$\text{NA} = n \sin \theta_{max} \tag{4.31}$$

$$\Delta x = 1.22 \frac{\lambda}{2 \sin \theta_{max}} = 1.22 \frac{\lambda n}{2 \, \text{NA}} \tag{4.32}$$

Resolution is fundamentaly different from magnification, since the magnification of the system (for example compound microscope) does not necessarily lead to better resolution. Sufficient magnification is however key to observe or record the image of given resolution and utilize resolution limit of the device.

In lensless optical systems, the maximum scattering angle is defined as the maximum angle, at which object produces an observable interference pattern at the detector [2]. The half-pitch resolution Δx is defined as

$$\Delta x = \frac{\lambda}{2 \, \text{NA}} = \frac{\lambda}{2n \sin \theta_{max}}. \tag{4.33}$$

Limitation by temporal coherence

The temporal coherence as desribed in 4.1.4 is a measure of how long a point in space stays at constant frequency (coherent), but this can also be seen from spatial perspective and measure for what distance in the propagation direction stays the wave coherent (longitudial coherence). This is definded by **coherence length** L_{coh} which can be computed as

$$L_{coh} = \left(\frac{2\ln 2}{\pi}\right)\frac{\lambda^2}{n\Delta\lambda} \tag{4.34}$$

where the **spectral bandwith** $\Delta\lambda$ is the primary limiting factor. [2]

From the coherence length, the maximum scattering angle and limit on coherence imposed by temporal resolution can be determined. [2]

$$\cos\theta_{max} \leq \frac{z}{z + L_{coh}} \tag{4.35}$$

$$\Delta x_{temporal} \geq \frac{\lambda}{2n\sin\theta_{max}} \tag{4.36}$$

where z is the reconstruction distance (object - sensor distance).

Limitation by spatial coherence and aperture smearing

The spatial coherence limitation is given by non-ideal point source dimensions. Since the point source is not exactly one spot, but rather a round aperture with diameter D, the waves originate from different points in space, which results in difference in optical path and subsequently phase delay. The aperture size D is (de)magnified by a factor of $M = \frac{z_1}{z_2} = \frac{L-z}{z}$ which improves the spatial coherence for $z_1 > z_2$. [2]

The maximum scattering angle and resolution limit are given by

$$\tan(\theta_{max}) \leq \frac{0.61\lambda}{D}\frac{z_1}{z_2}, \tag{4.37}$$

$$\Delta x_{spatial} \geq \frac{\lambda}{2n\sin\theta_{max}}. \tag{4.38}$$

This resolution limit is influenced mainly by the aperture size D and the relative choice of z_1 and z_2.

Another aspect that is influenced by aperture size and it's demagnification is the **spatial smearing**. This is induced by the illumination aperture

function T, which by convolution with the ideal coherent hologram smears the intensity function in the hologram plane (eqn. 4.39).

$$I_{hologram} = I_{coh} * T\left(-\frac{z_1}{z_2}x, -\frac{z_1}{z_2}y\right) \qquad (4.39)$$

Because of this, the illumination aperture must be de-magnified such that it is smaller than the pixel size and merges into the pixel function. [1]

Limitation by pixel size

If the design of the devide is well designed with respect to the properties of the light source, the only limiting factor to resolution of lensless inline digital holography is the pixel size. The finite pixel size introduces a limit on resolution, which is inversely proportional to magnification and proportional to the linear pixel size.

Important to note is that this pixel size limitation can be overcome by using any of the super-resolution techniques [38]. The techniques for super-resolution can be divided into software and hardware approaches. Software approaches rely on recovering sub-sampled information from original recording using analytical software solutions, for example, compressed sensing method [19]. The hardware approaches use multiple measurements (low-resolution images) that are combined into a single high-resolution image. There are numerous ways of creating and combining multiple measurements to obtain better resolution. The low-resolution images can be obtained by shifting the illumination aperture by sub-pixel distances [39], they can be obtained and combined by observing moving objects in a micro-fluidic channel [21], by wavelength scanning [40]. Arguably the most sophisticated approach is using the synthetic aperture [20], where the sample is scanned across different angles of illumination and the measurements combined in the frequency domain. With this approach resolution of $250\,nm$ and unit magnification was reported [20], corresponding to the best reported effective NA of digital inline holographic setup. However, this approach requires a complicated and expensive hardware setup.

Design of DLHM Device

With respect to the cost and potential applications, the digital lensless holographic microscope (DLHM) was selected as the focus of the practical lensless imaging implementation.

The objectives of the implementation were the following:

- decide on modifications of the camera module with CMOS imaging sensor

- design a simple 3D-printed optical setup

- decide on and realize the point source to achieve sufficient coherence and interference fringes

- reconstruct the original object wavefront at various depths

- realize graphical user interface

5.1 Hardware

The first step of the design was choosing the optimal available hardware to meet the coherence requirements of the inline holographic setup and the best possible resolution.

5.1.1 Image Sensor

The available image sensors are of two types - CCD (charged coupled device) or CMOS (complementary metal-oxide-semiconductor). The main differences between the two are in pixel size, signal-to-noise ratio (SNR), and commercial availability. CCD sensors achieve better SNR because in the CMOS sensor there is in each pixel more space occupied by other than light-sensing components. However, state-of-the-art CMOS sensors can be

fabricated with smaller pixel sizes, reaching even sub-micron pixel sizes compared to approx. $4\,\mu m$ with CCD. The CMOS sensors are benefiting from the development and manufacturing improvements of other electronics using the same technology in other markets (smartphones, computing communications, etc.), making them comparably cheaper [3].

Choice of Sensor for DLHM

The choice of the sensor type also depends on the application - whether high SNR or low pixel size and cost are more important. Because the design with a partially coherent light source was preferred and the setup uses no magnifying lenses, the major limit on the resolution is imposed by the pixel size. For this reason, the CMOS sensor is more suitable for the on-chip holographic device.

The choice of the specific device then follows firstly the minimal available pixel size criterium and secondly the largest possible sensor area/pixel count which directly determines the field-of-view of the device. Important to note is that the illumination is monochromatic so the monochromatic sensors are preferred and straight-forward to utilize for reconstruction. However, because most of the commercial applications and development are in the smartphone industry, most of the best available sensors are color sensors - sensors with Bayer color filter overlay.

Several camera modules were tested with appropriate imaging setups and the final choice of the sensor module was the **Raspberry-Pi Camera V2** with the sensor Sony IMX219, resolution of 3280×2464 pixels and pixel size $\mathbf{1.12\,\mu m \times 1.12\,\mu m}$. The reasons for this choice were the relatively small pixel size, availability of the sensor, comparably extensive documentation (relative to other used sensors), and software flexibility (compatible with camera read-out libraries for Raspberry-Pi). The drawback of this sensor was that this camera module has a color sensor, meaning there is a **Bayer color grid** (fig. 5.1) with a filter on each pixel that cannot be easily removed. Moreover, the color grid in this application created artifacts caused by demosaicing algorithms (reconstructing a color image from pixels of a different color).
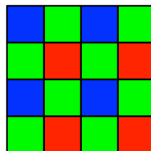

Figure 5.1: Color filters on pixels in Bayer grid [41]

Avoiding Demosaicing Artifacts

When the color image sensor was first used with a properly designed imaging setup to achieve sufficient coherence, the resulting image was of much lower resolution due to demosaicing algorithms. The illustration is shown in fig.5.2 where numbered centering electrodes on microscope glass are captured.
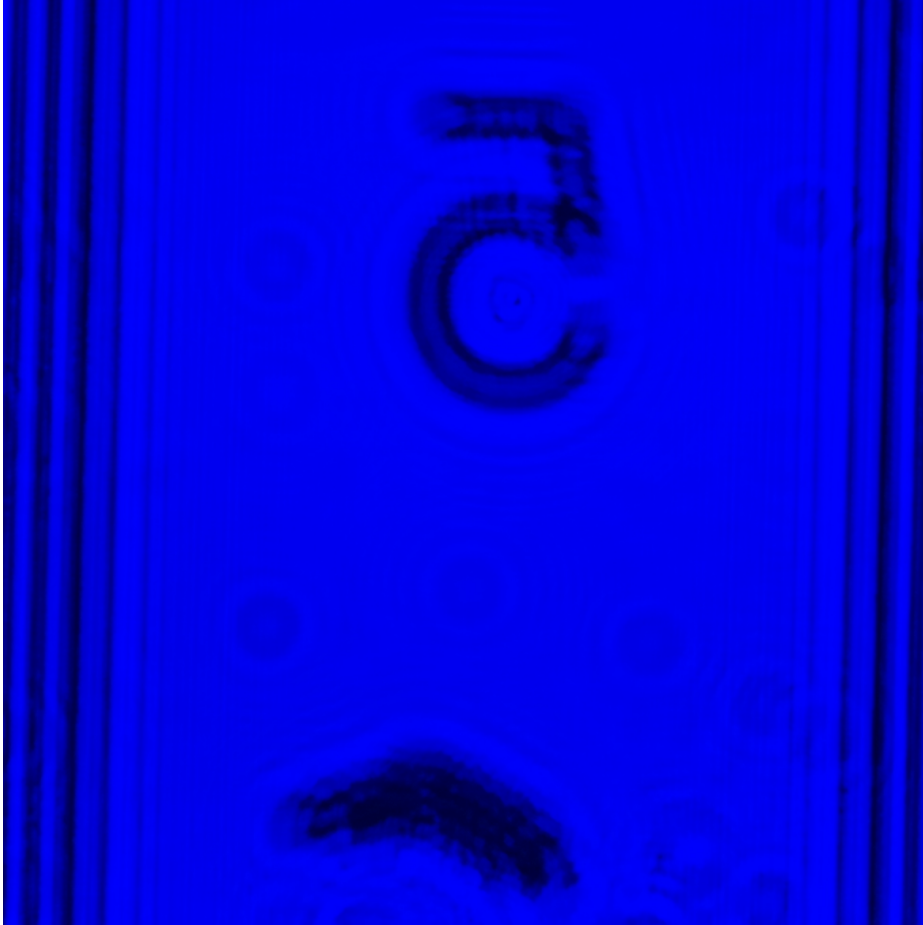

Figure 5.2: Almost totally smoothed interference fringes due to demosaicing. Imaging setup with blue LED illumination. Area of $1310\,\mu m \times 1310\,\mu m$.

These algorithms are used in the processing of the values from pixels under different color filters of the Bayer grid to get a single color image with RGB information for every pixel. The algorithms differ depending on the sensor, but always use some kind of averaging schema to achieve this goal. This is undesirable for holographic applications because it results in smoothing all or most of the interference fringes and making the reconstruction impossible.

One solution to this problem is by using only pixels with the filter of the same color. For this, it is necessary to use raw image information and

have documentation about the Bayer order for the given sensor. With the information about the metadata of the raw format and order of the pixels in the file, it is possible to **extract only every 4th pixel, corresponding to chosen color filter** (according to the wavelength of illumination). By doing this, the averaging over surrounding pixels was avoided and image quality improved (5.3). This also changes the (virtual) pixel size to be twice the single-pixel size $d_{px} = 2 \cdot 1.12\,\mu m$, determining the pixel size limit on achievable resolution. This information about the virtual pixel size is also an important parameter that is later used in the digital reconstruction.
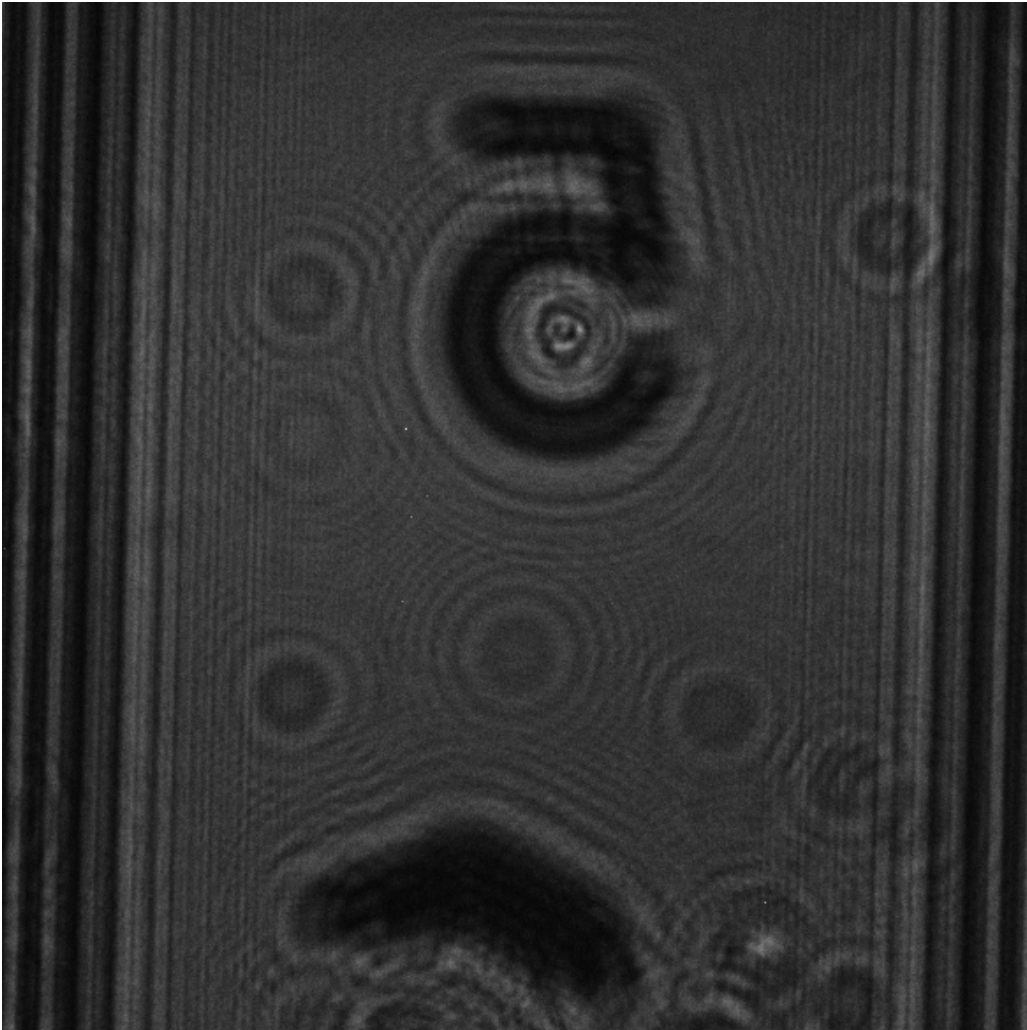
Figure 5.3: Hologram captured by using only every 4th pixel with differentiable interference fringes. Imaging setup with blue LED illumination. Area of $1310\,\mu m \times 1310\,\mu m$.

Even better resolution can be acquired if **both of the diagonal green pixels** from the square grid are used and then **rotated**. For this it is

necessary to use greed LED illumination (wavelength $\approx 500\,nm$ to $580\,nm$), because these pixels are less sensitive to illumination at other wavelengths (fig. 5.4).
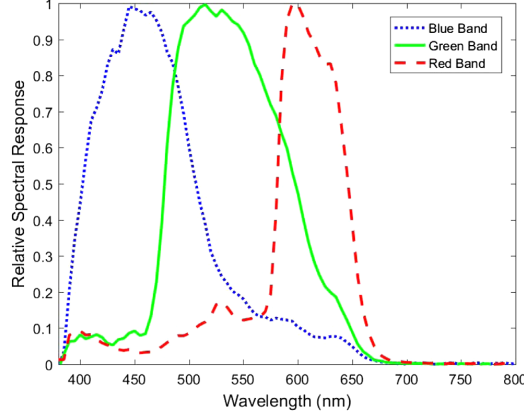
Figure 5.4: Spectral response of Raspberry-Pi Camera V2 [42]

Two images from the upper right and lower left green pixels are obtained and then combined to form an image of better resolution. The problem is that this image cannot be simply used for reconstruction with completely dark pixels on the other diagonal because that would disrupt the light back-propagation in the reconstruction. These empty pixels can either be filled with neighboring values (effectively averaging and worsening the image quality) or rotated according to fig. 5.5 to form a new virtual grid of pixel size $d_{px} = \sqrt{2} \cdot 1.12\,\mu m$.
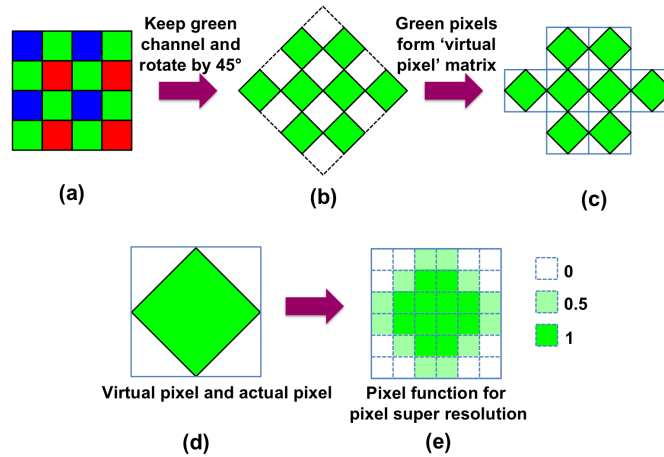
Figure 5.5: Rotation of only green pixels to create new image [41]

Apart from image processing, the image sensor module was also physically modified by removing the imaging lens mounted on the sensor and

41

striping all unnecessary parts to be able to place the observed sample as close as possible to the sensor. The physical design of the sensor and placement of the pixels under protection layers is unfortunately not always precisely specified and differ for every sensor. The smallest distance between the sample and sensor that was achieved in our setup with this sensor was 4 mm, which is not ideal and in combination with limited temporal coherence poses limitations on the final resolution.

5.1.2 Illumination

For any holographic setup, to get a hologram with distinguishable interference fringes, it is necessary to satisfy conditions for interference, namely temporal and spatial coherence (detailed description in Chapter 4).

Spectral Bandwith

Temporal coherence of the light source is specified by its spectral bandwidth. Insufficient temporal coherence results in worsening the resolution beyond the pixel size limitation or imposes additional restrictions on geometrical design. The **temporal coherence limitation on resolution** is related to the distance of the sample to the sensor so that if the spectral bandwidth is not sufficiently small, then the sample must be placed closer to the sensor. If that is no longer possible then the resolution will be limited beyond the pixel size.

The light source for these requirements can be realized with either light-emitting diode **(LED) coupled with narrow-band color filter** or with a laser diode (LD). The choice between LED and LD depends on the chosen optical setup, which can either be an on-chip design with the sample close to the sensor and far from the light source or with a sample close to the light source and far from the sensor in which case coherence requirements are high and LD is required.

In our case a combination of light-emitting diode (LED) with larger bandwidth was used in combination with a narrow-band color filter with a spectral bandwidth $\Delta\lambda = 20\,nm$ at the wavelenth $\lambda = 532\,nm$. Two different $5\,mW$ laser diodes were also tested, but not used in the final design due to alignment and brightness issues.

Aperture

Another important aspect of the holographic imaging design is a way of ensuring sufficient spatial coherence of the light source and creating a so-

called **point source**. The point source is an approximation in which the light source is considered to be infinitesimally small. In reality, the light source needs to be at least so small that the difference in optical path length between different parts of the light source is so small that the light wave can still be considered coherent.

This requirement implies that it is needed to use some kind of aperture (opaque barrier with a small hole etc.) to restrict the size of the original light source and there are numerous possibilities of implementing this.

The simplest way is to use a **metalic pinhole** of required size, depending on the the geometry of the optical setup. Again, the requirements for coherence is larger if the sample is placed close to the light source and in this case a pinhole of the size on the order of wavelength (micron or submicron size) is required. On the other hand, in an on-chip setup with a sample close to the sensor, the aperture is demagnified and it is sufficient to have an aperture of the size of $\approx 20\,\mu m - 200\,\mu m$. This implementation was used in our design, specifically a pinhole of size $25\,\mu m$ placed after the LED and color filter.

Figure 5.6: Pinhole used in DIHM design [43]

Another possibility that offers more variability in illumination design is using **optical fiber** coupled to LD or LED. The optical fibers are made in various diameters, single-mode fibers with a diameter $\approx 9\,\mu m$ to multimode fibers with diameter $50\,\mu m$ or more. The setup with optical fiber was also tested, but the coupling to the light source proved to be non-trivial and the non-professional connection resulted in a too-large light intensity loss at the end of the fiber.

The last explored option was the creation of the **point source using lenses**. In this case, the laser diode is collimated using one lens and focused using a second lens, forming a focal point, imitating the point source. The expanding wave after the focus point has properties that determine the NA of the light source and possible resolution [17]. There are a few examples

in the literature using GRIN [44] or aspheric lenses [17], which in the latter case allowed creating the cheapest point source so far for only 5.79 USD [17]. This imaging setup is still considered lensless since the lenses are not used for imaging itself, only to create the point source and thus the setup does not suffer from lens-based imaging limitations. This setup was tested but not used in the final design due to problems with high power intensity of laser diode illumination.

Apart from tested options, there is another way of creating the point source using engineered optical fiber [35]. The end of regular fiber tip or laser diode without additional elements are also producing a diverging beam that could serve as a point source itself, but their NA is not sufficiently high to ensure reasonable resolution. The fiber can be modified to have a **cone-shaped fiber tip**, which increases the NA so that it is possible to use it as a well-performing point source [35]. The creation of the point source using this method is also low-cost, but requires chemical etching procedure [45], which was not used on the optical fibers for our testing setup.

5.1.3 Platform

For the LED and image acquisition control was selected as a platform the Raspberry Pi 4, which was then also used for the reconstruction computations and GUI implementation. The control and computation scripts were written in Python. For the image acquisition, the Raspicam module was used and Picamraw Python package was used for the extraction of raw data from the sensor.

5.2 Design of Geometrical Parameters

After having the hardware selected, it is necessary to take into account the parameters of the sensor, the illumination, and other requirements to design optimal placement of all the elements to achieve the best possible resolution. In practice, this process was rather recursive with first, determining the hardware, then computing the geometry and determining the possible device performance and then modifying the hardware again to improve on the weak spots of the device.

Several parameters need to be considered for the geometry design and which are influencing the achievable resolution.
Firstly, there are parameters of CMOS sensor:

- the pixel size p

- the pixel count N (number of pixels in x or y direction)

- signal-to-noise ratio

- Bayer color matrix (in non-monochromatic sensors)

The pixel size influences how closely spaced fringes in the sensor plane can still be distinguished and is the main limiting factor of digital inline holographic microscopy with the sample placed closed to the sensor. The pixel count determines the Field of View of the device - how large an area can be imaged at once.

Secondly, the resolution depends on light source parameters. Parameters are as follows:

- pinhole size D

- illumination wavelength λ

- LED power (to achieve sufficient power density at the sensor plane)

Thirdly, the geometrical parameters of DLHM setup are the distance from the point source to the sensor (L) and the distance from the sensor to the sample (z). The ratio of these distances can be used to our the advantage in two ways, by improving the illumination coherence or by magnifying the image.

5.2.1 Geometry Design Algorithm

The several introduced limiting factors to the hologram resolution are interconnected, but to determine the geometrical parameters, they were decomposed to create a step-by-step design algorithm. Firstly there is a sampling limitation by pixel size, which depends on the image sensor's characteristics. It is desirable to have the smallest possible pixel size and monochromatic sensor. State-of-the-art sensors are available with a pixel size slightly below $1\,\mu m$. With this limitation in place, all of the other system parts should ideally, be designed in such a way that limitation imposed by both temporal and spatial coherence are below the pixel size and do not further decrease the achievable resolution.

The temporal coherence limitation is influenced by the bandwidth of the light source and the distance of the sample from the sensor plane. In the case of a laser diode as a light source, this limitation is negligible due to the sufficient temporal coherence of the laser. However, in the case of an LED

light source, this is usually the main source of a decrease in resolution. The coherence length ΔL_c is defined as:

$$\Delta L_c \approx \frac{2\ln(2)}{\pi} \cdot \frac{\lambda^2}{n \cdot \Delta\lambda} \qquad (5.1)$$

where λ is source wavelength. Then from this, maximum scattering angle can be computed (maximum angle at which scattered waves contribute to the hologram).

$$\cos(\Theta_{max}) = \frac{z}{z + \Delta L_c} \qquad (5.2)$$

$$\Theta_{max} = \arccos \frac{z}{z + \frac{2\ln(2)}{\pi} \cdot \frac{\lambda^2}{n \cdot \Delta\lambda}} \qquad (5.3)$$

And finally the resolution limit due to limited temporal coherence is:

$$\Delta x = \frac{\lambda}{2NA} = \frac{\lambda}{2n\sin(\Theta_{max})} \qquad (5.4)$$

$$\Delta x = \frac{\lambda}{2n\sin\arccos\frac{z}{z + \frac{2\ln(2)}{\pi} \cdot \frac{\lambda^2}{n \cdot \Delta\lambda}}} \qquad (5.5)$$

where n is refractive index of the medium, in our case $n = 1$. Resolution can be improved (Δx decreased) with the decrease in wavelength and bandwith (with the use of color filter) and by decrease of distance z between sensor and sample to the point where the resolution limit imposed by temporal coherence is bellow the pixel size. In the case where the distance z is limited by the construction of the sensor or other requirements and the temporal resolution, limit is above pixel size, it is necessary to use a filter with narrower bandwidth, LED with lower wavelength or switch to a laser diode. Otherwise, the resolution will be below the possibilities of the sensor.

In the case of our setup, the virtual pixel size is $D_{px} = 2.24\,\mu m$, mean wavelength $\lambda = 532\,nm$, spectral bandwith $\Delta\lambda = 10\,nm$ and minimal possible distance from sensor to sample $z = 4\,mm$ Resulting resolution limit posed by temporal coherence limitation is $\Delta x = 3.37\,\mu m$

If the bandwidth, wavelength, and distance from the sample to sensor (z) are selected, the last the step is to choose the right distance L from the sensor to the light source to ensure sufficient spatial coherence and reduce spatial smearing. This means, that the aperture diameter (in our case pinhole size) needs to be demagnified so that its projection is below the pixel size (or below the limitation by temporal coherence which might be greater than pixel size). The demagnification factor of the aperture is $\frac{1}{M} = \frac{z}{L-z}$ and the goal is to make L large enough to sufficiently demagnify aperture size to be

bellow the pixel size (or previous resolution limit if greater than pixel size)

$$D \cdot \frac{1}{M} < D_{lim} \tag{5.6}$$

$$D \cdot \frac{L - z}{z} > D_{lim} \tag{5.7}$$

$$L > \left(\frac{D_{lim}}{D} + 1 \right) z \tag{5.8}$$

In our setup, the resolution limit due to temporal coherence $\Delta x = 3.37\,\mu m$ is greater than the virtual pixel size $D_{px} = 2.24\,\mu m$. The goal of demagnification is thus an aperture of size $D_{lim} = 3.37\,\mu m$. The aperture size of pinhole is $D = 25\,\mu m$ and minimal distance from sensor to sample $z = 4mm$. From this, the minimal L (source - sensor) distance can be computed as $L_{min} \approx 34\,mm$.

The 3D model of the setup was created according to the computed parameters and printed on a Prusa MK3S 3D printer. The final device (without Raspberry Pi) is shown in figure 5.7. At the bottom there is the LED, controlled by the Raspberry Pi, just above the LED is a color filter and the metallic pinhole. At the top, there is the image sensor module, connected to the Raspberry Pi and directly bellow the sensor, there is inserted the observed sample (numbered centering electrodes in this case). The device is designed in closed form to block outside light from the imaging area.
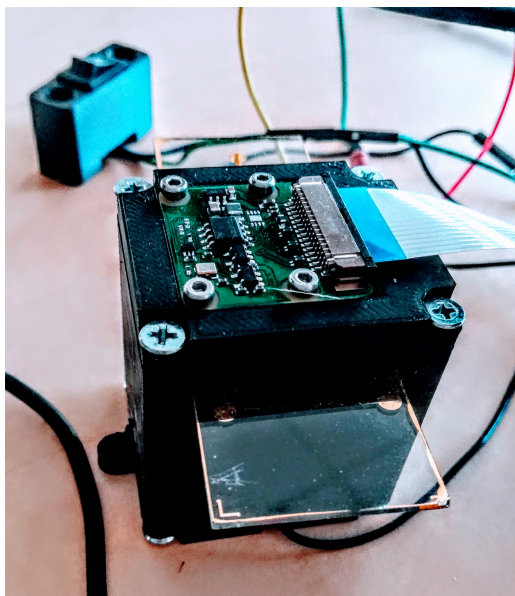
Figure 5.7: 3D printed DLHM device

5.3 Reconstruction Algorithm

At first, two tools for holographic reconstruction were explored, namely, the HoloPy library for Python [46] and Unal-optodigital's Digital Holographic Microscopy plugin for ImageJ [47] with the second performing faster reconstruction.

For the reconstruction computation on Raspberry Pi, the method for angular spectrum field back-propagation (chapter 4.2.3) was implemented in Python using the Numpy library. First the grid of Fourier frequencies f_z based on pixel dimensions in x and y dimensions are created. After that the 2D Fourier transform of the hologram $\mathcal{F}\{E_0\}$ is computed as well as the Fourier image of the impulse response of free space propagation $\mathcal{F}\{h\}$ (based on the the wavelength of the illumination, reconstruction distance, and sensor characteristics). Then the inverse 2D Fourier transform is performed on the convolution (product in Fourier domain) of the E_0 and h to get the back-propagated complex amplitude of electric field in the distance z (specified reconstruction distance). The computation time of a single image at one reconstruction distance was roughly 2s at the Raspberry Pi 4 with.

5.4 Graphical User Interface

A graphical user interface (GUI) was created with Tkinter Python package to be used on Raspberry-Pi 4 with a display of resolution $800 \times 600\,px$. The interface first offers the user a choice of setup parameters, such as illumination wavelength, pixel size (virtual pixel size), expected distance of the object from the sensor (later will be adjusted by refocusing to other distances), shutter time and preferred preview time before the image capture.

After that, a new window opens, where the user can view the reconstructed amplitude image, refocus to other distances by pressing buttons $\pm 10\,\mu m$ or $\pm 100\,\mu m$ and zoom in on the image. The reconstructed images are saved in a dictionary so that the previously computed reconstructions do not have to be performed again.

In the end, the selected reconstruction image or complete stack of reconstruction, images can be saved to local memory on the device.
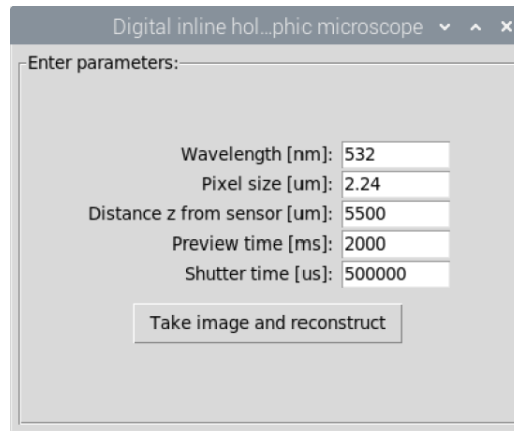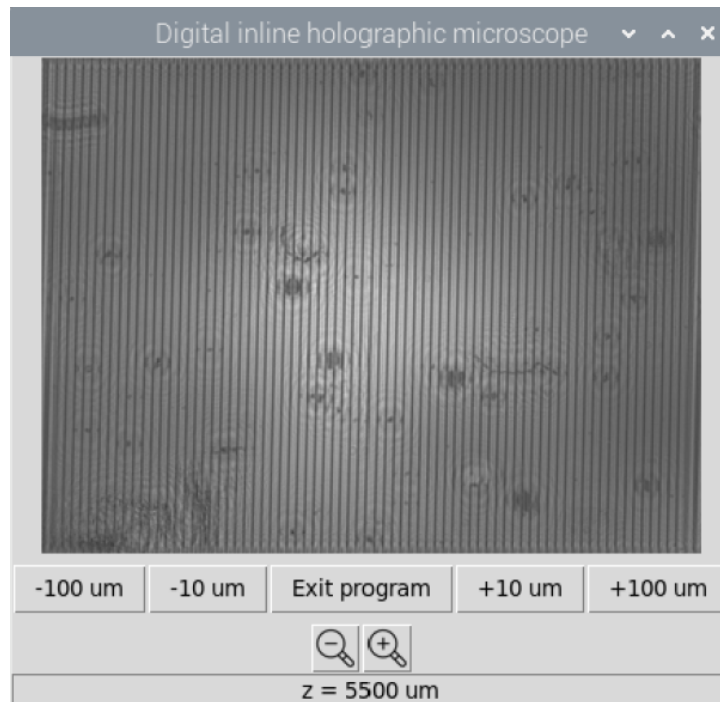
Figure 5.8: GUI selection of parameters


Figure 5.9: GUI reconstruction menu

5.5 Experimental Results

5.5.1 Yeast Cells

The designed DLHM device was tested for its ability to image yeast cells sample. The diameter of the cells varies between $3-4\,\mu m$. The in-focus reconstruction distance was found at $5400\,\mu m$ from the sensor. For better clarity, section A of the original image was cropped, images 5.10b and 5.10c are created from this section. The total imaging area of the sensor is $3.6736\,mm \times 2758.7\,mm = 10.137\,mm^2$. The real size of objects in the sample plane depends on the magnification, given by the distance of the sensor to the sample and the light source. In this case for the reconstructed area A from the original figure has real dimensions of $0.563\,mm \times 0.563\,mm = 0.315\,mm^2$. The yeast cells can be easily resolved.
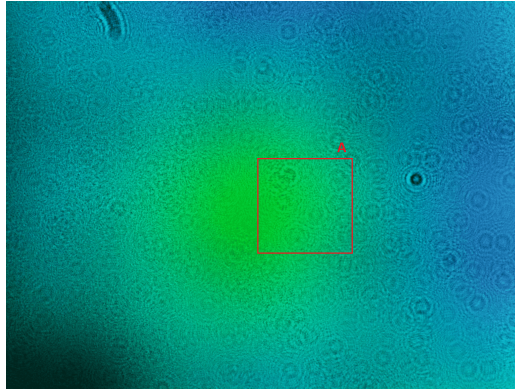
(a) Yeast cells - Original raw image hologram
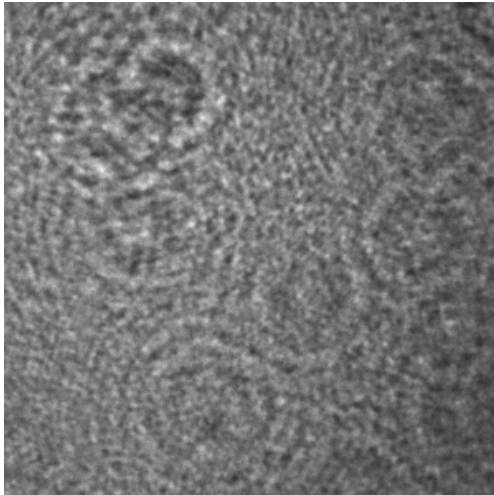
(b) Hologram using every 4th pixel
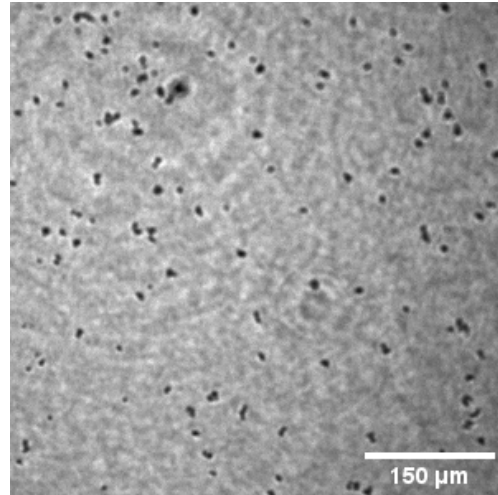
(c) Reconstruction at distance $5400\,\mu m$

Figure 5.10: Yeast cells - hologram and reconstruction

5.5.2 Numbers on Centering Electrodes

As a convenient tool for demonstrating and testing the reconstruction quality, numbers on centering electrodes were used as the sample objects. The thickness of the font line of the numbers was measured to be $40\,\mu m$. Grating on the sides has a thickness of $15\,\mu m$ and spacing of $25\,\mu m$. Both of these can be easily resolved in figure 5.11c.
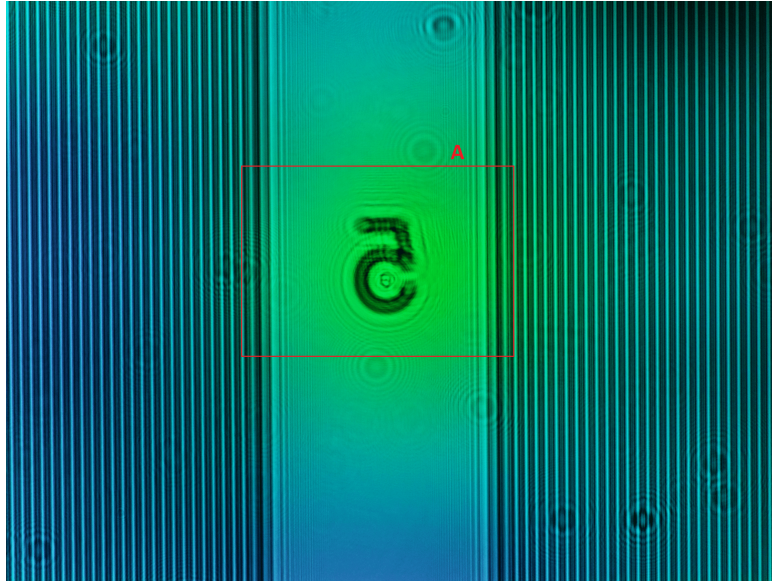
(a) Yeast cells - Original raw image hologram
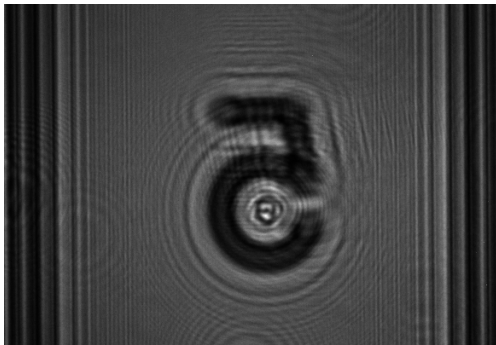
(b) Hologram using every 4th pixel
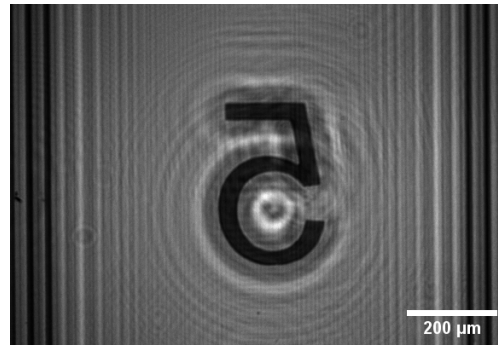
(c) Reconstruction at distance $5500\,\mu m$

Figure 5.11: Electrodes - hologram and reconstruction

5.5.3 Comparing Different Illumination Wavelengths

The green LED illumination was originally used to utilize both green pixels and creating a diagonally rotated hologram with virtual pixel size of $\sqrt{2} \cdot 1.12\,\mu m$. In the end, the limitation imposed by temporal coherence restricted resolution beyond $3\,\mu m$ and effectively erased differences between using every 4th pixel with a virtual pixel size of $2 \cdot 1.12\,\mu m$ or by using both diagonal pixels with virtual pixel size $\sqrt{2} \cdot 1.12\,\mu m$. Since the temporal coherence is also influenced by the illumination wavelength, the green LED illumination ($532\,nm$) was compared in the same setup with blue LED illumination ($470\,nm$). In the reconstruction in In both cases only every 4th pixel of the raw image was used, so that the virtual pixel size was $2.24\,\mu m$ in both cases.

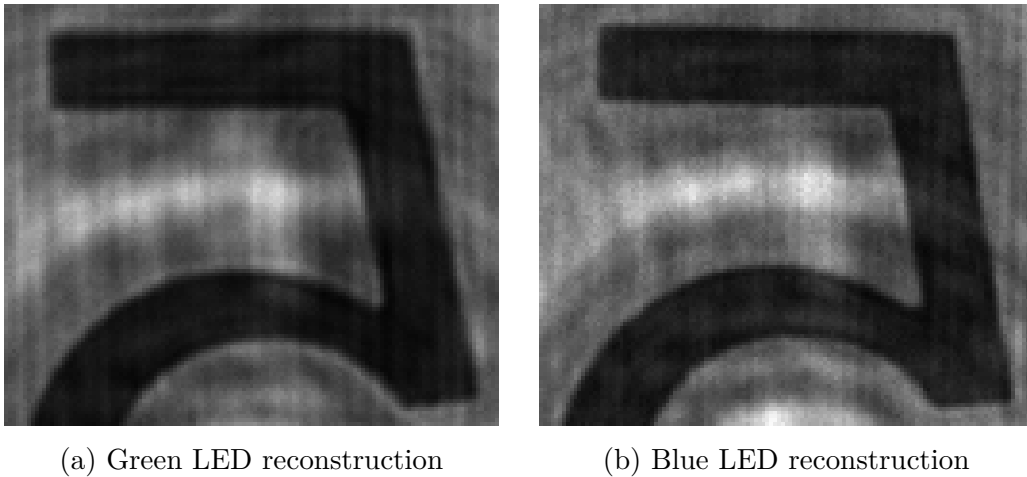(a) Green LED reconstruction   (b) Blue LED reconstruction

Figure 5.12: Comparison of resolution of blue and green LED

The comparison in image 5.12 showed slightly better resolution for blue LED illumination of shorter wavelength, suggesting that the resolution was indeed limited by the temporal coherence of the light source and not by the pixel size. If the temporal coherence were not a limiting factor, both images should have the same resolution.

5.5.4 Axial Scanning

The last section demonstrates the effects of focusing at different depths of the image. This is done by propagating the wave digitally to different depths (using the same hologram) and as a result objects at different depths come into focus when the wavefront is propagated to its original positions.
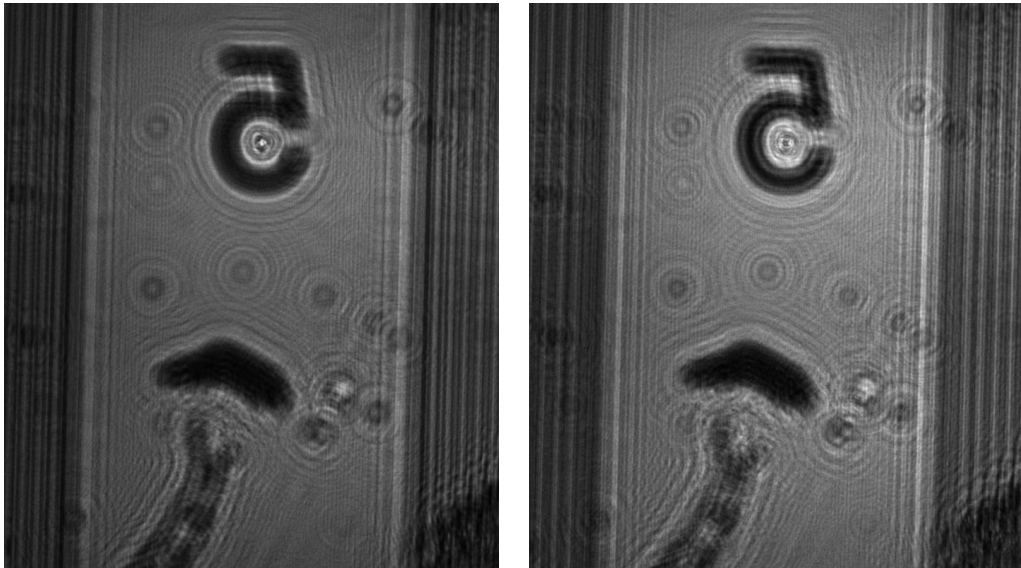
(a) Reconstruction at distance $2000\,\mu m$

(b) Reconstruction at distance $3000\,\mu m$
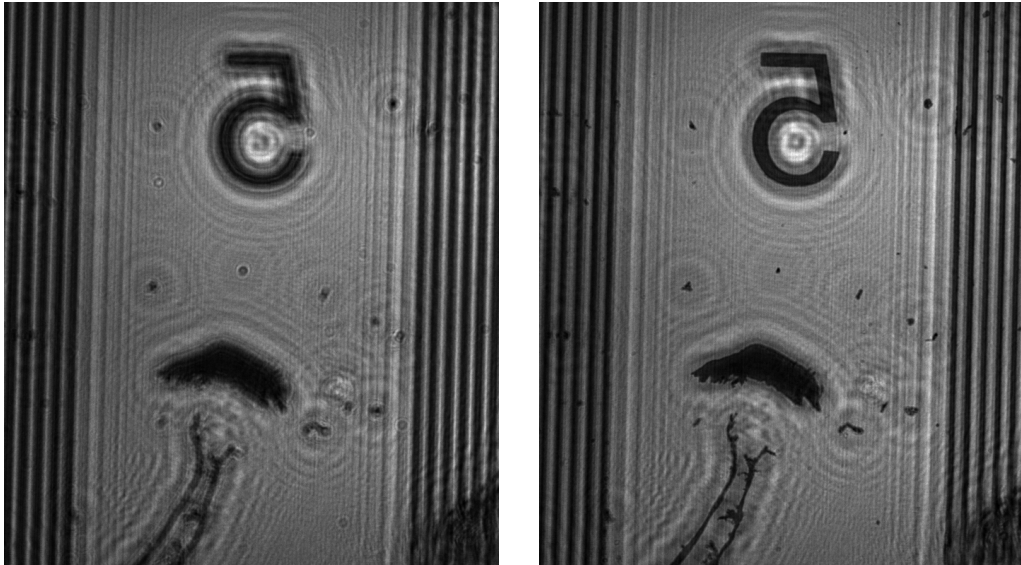
(c) Reconstruction at distance $5000\,\mu m$

(d) Reconstruction at distance $5500\,\mu m$

Figure 5.13: Reconstruction at different distances from the sensor

5.6   Summary and Further Improvements

Design Summary

The device was designed according to the theory to best reflect the design objectives of best possible resolution, simplicity and close to real-time reconstruction. The technology of choice was digital holography in in-line configuration with partially-coherent illumination.

The hardware choices and geometrical parameters of the design were made in order to minimize the spatial and temporal coherence resolution limitations and best utilize the available Raspberry-Pi Camera V2 module with a pixel size of $1.12\,\mu m$ and Bayer color grid. Due to restrictions of the sensor module's housing, the sample was placed at further than the optimal distance from the sensor, resulting in temporal coherence limited resolution of the setup. This was demonstrated in an experiment, showing different resolution at different illumination wavelengths, a phenomenon that would not be observable if the resolution was limited only by pixel sampling.

According to the theoretical design computations, the resolution of the device should be $3.37\,\mu m$ with illumination at $532\,nm$. The final experimental resolution was not rigorously tested, but the ability to image yeast cells was demonstrated, suggesting that the final resolution is in the expected range. With this resolution, it is possible to use the device in lab-on-a-chip applications, for routine sample inspections, in simple tomography or in cell tracking applications.

Further Improvements

Apart from the basic reconstruction and physical design, the device could be expanded according to preferred use-cases.

In the current design, only amplitude information was reconstructed, but the device could be further improved by recovering also the **phase information** for imaging of transparent samples. This step would require an iterative phase recovery algorithm that would significantly increase the computation time so that a more efficient implementation of the propagation algorithm would likely be required using either GPU computation, implementation in other programming language or possibly deep-learning reconstruction.

The hologram recording could also be extended to allow video capture, reconstructing stack of images at different moments and **tracking movements** of the particles in the sample.

The **resolution** of the device could also be further improved (up to $\sqrt{2} \cdot 1.12 \, \mu m$) by modifying the sensor housing and placing the sample closer to the sensor and using the already implemented algorithm for utilizing both of the diagonal green pixels of the Bayer grid. Another resolution improvement could be achieved using the software super-resolution algorithms.

Conclusion

Various lensless imaging technologies were introduced as well as their benefits, drawbacks and potential applications. The described technologies are not completely new, but many use-cases have first been possible and affordable in the last few years thanks to continued CMOS sensors development, 3D print expansion and advances in other technologies utilized in the lensless imaging devices. As such, this field is very promising for the future of imaging in biology, medicine, environmental monitoring, and many other fields.

In this thesis, a design of a digital lensless holographic microscope was presented step-by-step from choosing the hardware, designing the geometrical parameters for 3D printed microscope housing and implementing the reconstruction and image processing algorithms. The necessary parts of physics were also summarized in order to theoretically support the design decisions and estimate the performance of the microscope.

The final device was tested on various samples to demonstrate the experimental resolution performance. The resolution capability was demonstrated on imaging of yeast cells with a diameter of $3 - 4\,\mu m$, corresponding to the theoretically suggested resolution limit of $3.37\,\mu m$. The device was also supplemented with a graphical user interface for control, computation, and visualization.

Possible extensions and improvements were suggested for the current design in the last chapter, including particle tracking, super-resolution and phase recovery algorithms.

List of Figures

Bibliography

[1] Y. Wu and A. Ozcan, "Lensless digital holographic microscopy and its applications in biomedicine and environmental monitoring," *Methods*, vol. 136, pp. 4–16, oct 2018.

[2] A. Ozcan and E. McLeod, "Lensless Imaging and Sensing," *Annual Review of Biomedical Engineering*, vol. 18, pp. 77–102, oct 2016.

[3] L. C. P. Gouveia and B. Choubey, "Advances on CMOS image sensors," *Sensor Review*, vol. 36, no. 3, pp. 231–239, jun 2016.

[4] A. F. Coskun and A. Ozcan, "Computational imaging, sensing and diagnostics for global health applications," *Current Opinion in Biotechnology*, vol. 25, pp. 8–16, feb 2014.

[5] A. Veeraraghavan, J. T. Robinson, L. Waller, and V. Boominathan, "Recent advances in lensless imaging," *Optica, Vol. 9, Issue 1, pp. 1-16*, vol. 9, no. 1, pp. 1–16, jan 2022.

[6] Z. Göröcs, Y. Ling, M. D. Yu, D. Karahalios, K. Mogharabi, K. Lu, Q. Wei, and A. Ozcan, "Giga-pixel fluorescent imaging over an ultra-large field-of-view using a flatbed scanner," *Lab on a Chip*, vol. 13, no. 22, pp. 4460–4466, oct 2013.

[7] Y. Fang, N. Yu, R. Wang, and D. Su, "An on-chip instrument for white blood cells classification based on a lens-less shadow imaging technique," *PLOS ONE*, vol. 12, no. 3, p. e0174580, mar 2017.

[8] S. A. Lee, X. Ou, J. E. Lee, and C. Yang, "Chip-scale fluorescence microscope based on a silo-filter complementary metal-oxide semiconductor image sensor," *Optics letters*, vol. 38, no. 11, p. 1817, jun 2013.

[9] A. F. Coskun, I. Sencan, T. W. Su, and A. Ozcan, "Wide-field lensless fluorescent microscopy using a tapered fiber-optic faceplate on a chip," *Analyst*, vol. 136, no. 17, pp. 3512–3518, aug 2011.

[10] B. Khademhosseinieh, I. Sencan, G. Biener, T. W. Su, A. F. Coskun, D. Tseng, and A. Ozcan, "Lensfree on-chip imaging using nanostructured surfaces," *Applied Physics Letters*, vol. 96, no. 17, p. 171106, apr 2010.

[11] R. Horaud, M. Hansard, G. Evangelidis, and C. Ménier, "An overview of depth cameras and range scanners based on time-of-flight technologies," *Machine Vision and Applications*, vol. 27, no. 7, pp. 1005–1020, oct 2016.

[12] V. Boominathan, J. K. Adams, J. T. Robinson, and A. Veeraraghavan, "PhlatCam: Designed Phase-Mask Based Thin Lensless Camera," *IEEE Transactions on Pattern Analysis and Machine Intelligence*, vol. 42, no. 7, pp. 1618–1629, jul 2020.

[13] R. Feynman, G. Michael, and R. Pfeiffer, "The Feynman Lectures on Physics Vol. I Ch. 31: The Origin of the Refractive Index," 1963. [Online]. Available: https://www.feynmanlectures.caltech.edu/

[14] U. Schnars, C. Falldorf, J. Watson, and W. Jüptner, *Digital holography and wavefront sensing: Principles, techniques and applications*, 2nd ed. Springer Berlin Heidelberg, 2015.

[15] D. Gabor, "A new microscopic principle," *Nature*, vol. 161, no. 4098, pp. 777–778, 1948.

[16] J. K. Adams, V. Boominathan, B. W. Avants, D. G. Vercosa, F. Ye, R. G. Baraniuk, J. T. Robinson, and A. Veeraraghavan, "Single-frame 3D fluorescence microscopy with ultraminiature lensless FlatScope," *Science Advances*, vol. 3, no. 12, 2017.

[17] C. Buitrago-Duque, E. Zora-Guzmán, H. Tobon-Maya, J. Garcia-Sucerquia, and S. Zapata-Valencia, "Open-source, cost-effective, portable, 3D-printed digital lensless holographic microscope," *Applied Optics, Vol. 60, Issue 4, pp. A205-A214*, vol. 60, no. 4, pp. A205–A214, 2021.

[18] J. Garcia-Sucerquia, "Color digital lensless holographic microscopy: laser versus LED illumination," *Applied Optics*, vol. 55, no. 24, p. 6649, aug 2016.

[19] J. Song, C. Leon Swisher, H. Im, S. Jeong, D. Pathania, Y. Iwamoto, M. Pivovarov, R. Weissleder, and H. Lee, "Sparsity-Based Pixel Super Resolution for Lens-Free Digital In-line Holography," *Scientific Reports 2016 6:1*, vol. 6, no. 1, pp. 1–9, apr 2016.

[20] W. Luo, A. Greenbaum, Y. Zhang, and A. Ozcan, "Synthetic aperture-based on-chip microscopy," *Light: Science & Applications 2015 4:3*, vol. 4, no. 3, pp. e261–e261, mar 2015.

[21] W. Bishara, H. Zhu, and A. Ozcan, "Holographic opto-fluidic microscopy," *6. R. Oosterbroek, Lab-on*, vol. 77, no. 3, p. 27499, 2010.

[22] A. C. Sobieranski, F. Inci, H. C. Tekin, M. Yuksekkaya, E. Comunello, D. Cobra, A. von Wangenheim, and U. Demirci, "Portable lensless wide-field microscopy imaging platform based on digital inline holography and multi-frame pixel super-resolution," *Light: Science & Applications 2015 4:10*, vol. 4, no. 10, pp. e346–e346, oct 2015.

[23] S. K. Jericho, P. Klages, J. Nadeau, E. M. Dumas, M. H. Jericho, and H. J. Kreuzer, "In-line digital holographic microscopy for terrestrial and exobiological research," *Planetary and Space Science*, vol. 58, no. 4, pp. 701–705, oct 2010.

[24] D. J. Brady, K. Choi, D. L. Marks, R. Horisaki, and S. Lim, "Compressive Holography," *Optics Express, Vol. 17, Issue 15, pp. 13040-13049*, vol. 17, no. 15, pp. 13 040–13 049, jul 2009.

[25] S. O. Isikman, W. Bishara, U. Sikora, O. Yaglidere, J. Yeah, and A. Ozcan, "Field-portable lensfree tomographic microscope," *Lab on a Chip*, vol. 11, no. 13, pp. 2222–2230, jun 2011.

[26] S. O. Isikman, W. Bishara, S. Mavandadi, F. W. Yu, S. Feng, R. Lau, and A. Ozcan, "Lens-free optical tomographic microscope with a large imaging volume on a chip," *Proceedings of the National Academy of Sciences of the United States of America*, vol. 108, no. 18, 2011.

[27] E. Hecht, *Optics: A Contemporary Approach to Optics with Practical Applications and New Focused Pedagogy, Global edition*, 5th ed.   Pearson, 2017.

[28] P. Picart, "Holography : Recording/Reconstruction," 2007. [Online]. Available: http://www.optique-ingenieur.org/en/courses/

[29] T.-C. Poon and J.-P. Liu, *Introduction to Modern Digital Holography: With Matlab.*   Cambridge University Press, 2014.

[30] Z. Gorocs and A. Ozcan, "On-chip biomedical imaging," *IEEE Reviews in Biomedical Engineering*, vol. 6, pp. 29–46, 2013.

[31] J. Garcia-Sucerquia, W. Xu, S. K. Jericho, P. Klages, M. H. Jericho, and H. J. Kreuzer, "Digital in-line holographic microscopy," *Applied Optics, Vol. 45, Issue 5, pp. 836-850*, vol. 45, no. 5, pp. 836–850, feb 2006.

[32] M. H. Jericho and H. J. Kreuzer, "Point source digital in-line holographic microscopy," pp. 3–30, 2011.

[33] K. Matsushima and T. Shimobaba, "Band-Limited Angular Spectrum Method for Numerical Simulation of Free-Space Propagation in Far and

Near Fields," *Optics Express, Vol. 17, Issue 22, pp. 19662-19673*, vol. 17, no. 22, pp. 19 662–19 673, oct 2009.

[34] J. R. Fienup, "Phase retrieval algorithms: a comparison," *Applied Optics, Vol. 21, Issue 15, pp. 2758-2769*, vol. 21, no. 15, pp. 2758–2769, aug 1982.

[35] B. Patiño-Jurado, J. Garcia-Sucerquia, and J. F. Botero-Cadavid, "Cone-shaped optical fiber tip for cost-effective digital lensless holographic microscopy," *Applied Optics, Vol. 59, Issue 10, pp. 2969-2975*, vol. 59, no. 10, pp. 2969–2975, apr 2020.

[36] S. O. Isikman, W. Bishara, O. Mudanyali, I. Sencan, T. W. Su, D. K. Tseng, O. Yaglidere, U. Sikora, and A. Ozcan, "Lensfree On-Chip Microscopy and Tomography for Bio-Medical Applications," *IEEE journal of selected topics in quantum electronics : a publication of the IEEE Lasers and Electro-optics Society*, vol. 18, no. 3, p. 1059, 2011.

[37] M. Born, E. Wolf, A. B. Bhatia, P. C. Clemmow, D. Gabor, A. R. Stokes, A. M. Taylor, P. A. Wayman, and W. L. Wilcock, *Principles of Optics: Electromagnetic Theory of Propagation, Interference and Diffraction of Light*, 7th ed.   Cambridge University Press, oct 1999.

[38] M. M. Khattab, A. M. Zeki, A. A. Alwan, A. S. Badawy, and L. S. Thota, "Multi-Frame Super-Resolution: A Survey," *2018 IEEE International Conference on Computational Intelligence and Computing Research, ICCIC 2018*, dec 2018.

[39] W. Bishara, T.-W. Su, A. F. Coskun, A. Ozcan, W. Haddad, D. Cullen, H. Solem, J. Longworth, A. McPherson, K. Boyer, and C. Rhodes, "Lensfree on-chip microscopy over a wide field-of-view using pixel super-resolution," *Optics Express, Vol. 18, Issue 11, pp. 11181-11191*, vol. 18, no. 11, pp. 11 181 – 11 191, 2010.

[40] W. Luo, Y. Zhang, A. Feizi, Z. Göröcs, and A. Ozcan, "Pixel super-resolution using wavelength scanning," *Light: Science & Applications 2016 5:4*, vol. 5, no. 4, pp. e16 060–e16 060, dec 2015.

[41] S. O. Isikman, A. Greenbaum, W. Luo, A. F. Coskun, and A. Ozcan, "Giga-Pixel Lensfree Holographic Microscopy and Tomography Using Color Image Sensors," *PLOS ONE*, vol. 7, no. 9, p. e45044, sep 2012.

[42] M. A. Pagnutti, R. E. Ryan, G. J. C. V, M. J. Gold, R. Harlan, E. Leggett, and J. F. Pagnutti, "Laying the foundation to use Raspberry Pi 3 V2 camera module imagery for scientific and engineering purposes," *Journal of Electronic Imaging*, vol. 26, no. 1, p. 013014, feb 2017.

[43] "Thorlabs - P25K Ø1" Mounted Pinhole, 25 $\pm$ 2 μm Pinhole Diameter, Stainless Steel." [Online]. Available: https://www.thorlabs.com/thorproduct.cfm?partnumber=P25K

[44] C. Lindensmith, E. Serabyn, J. Nadeau, K. Wallace, and K. Liewer, "Compact, lensless digital holographic microscope for remote microbiology," *Optics Express, Vol. 24, Issue 25, pp. 28540-28548*, vol. 24, no. 25, pp. 28 540–28 548, dec 2016.

[45] B. A. Puygranier and P. Dawson, "Chemical etching of optical fibre tips - Experiment and model," *Ultramicroscopy*, vol. 85, no. 4, pp. 235–248, dec 2000.

[46] S. Barkley, T. G. Dimiduk, J. Fung, D. M. Kaz, V. N. Manoharan, R. McGorty, R. W. Perry, and A. Wang, "Holographic Microscopy with Python and HoloPy," *Computing in Science and Engineering*, vol. 22, no. 5, pp. 72–82, sep 2020.

[47] C. Buitrago-Duque and J. Garcia-Sucerquia, "Realistic simulation and real-time reconstruction of digital holographic microscopy experiments in ImageJ," *Applied Optics, Vol. 61, Issue 5, pp. B56-B63*, vol. 61, no. 5, pp. B56–B63, feb 2022.